1954

Analysis and tests of a cylindrical shell roof model., Proc. ASCE Separate No. 434, 1954, Reprint No. 95 (54-2)

B. Thurlimann

B. G. Johnston

ANALYSIS AND TESTS OF A CYLINDRICAL SHELL ROOF MODEL

by

Bruno Thürlimann *

and

Bruce G. Johnston**

Fritz Engineering Laboratory Report 213K

Synopsis:

Analytical expressions for the effective width of cylindrical shells, adjacent to stiffening ribs in circumferential direction, are presented. Use of these formulas is made for the analysis of a cylindrical shell roof acted upon by horizontal longitudinal forces. Furthermore, the influence of foundation movements, temperature changes, and shrinkage is studied.

The theoretical results are compared with experimental measurements obtained on a model in the approximate scale 1 to 30 of an actual cylindrical shell roof. Good agreement between analysis and test is established.

Introduction:

It is often believed that the use of shells as structural elements is a modern development. But two thousand years ago the Romans already admired their Pantheon, a building covered by a spherical shell of about 145 ft. diameter. The cupolas of the cathedrals of Florence and St. Peter in Rome, built during the 15th and 16th century respectively and having a diameter of about 140 ft, are examples of remarkable craftmanship, based on experience and intuition only. The contribution of our age to this type of structures consists in developing a rational analysis

---

*Former Research Engineer, Fritz Engineering Laboratory, Lehigh University, Bethlehem, Pa.

**Professor of Structural Engineering, Civil Engineering Dept., University of Michigan, Ann Arbor, Michigan, formerly Director of Fritz Engineering Laboratory, Lehigh University, Bethlehem, Pa.

predicting sufficiently close the state of forces in the shell.

The development of the "Shell Theory" was initiated by Love (1)* who derived the differential equations for curved plates. Meissner (2) succeeded in integrating these equations for spherical and conical shells. Bauernsfeld's (3), Finsterwalder's (4), and Dischinger's (5) contributions made an application of the theory to the analysis of actual structures possible. A number of shells in reinforced concrete were built in Europe after the first world war and parallel to this development important theoretical contributions were made.

It was the Roberts and Schaefer Company, Chicago, Illinois who introduced this promising type of structure in the United States. The Ice Arena in Hershey, Pennsylvania, 1936 (6)**, was the first cylindrical shell roof in the United States. In the following years and especially during and after the war, this company was designing a number of shell roofs used as storage houses, factory buildings, airplane hangars, sport arenas, armories, etc., covering a total of ten million sq. ft.

Today the largest span of cylindrical shell roofs arrived at is 340 ft. (e.g. Hangars at Rapid City, South Dakota (7), and Limestone, Maine (8)). These large span structures accentuated certain problems which were of secondary importance in the smaller structures, built previously. Furthermore, the tendency is toward an increase of the span, so that a careful study of these the following questions became mandatory. ~~The slenderness of~~

*For list of references see p. 31.

**Ref. (6) outlines the principles of shell structures and gives a number of actual examples.

"The supporting ribs in cylindrical shell roofs may be designed as tee sections to include the additional effective section provided by the shell. A study[16] of the interaction between the ribs and shell shows that an "effective width" of shell can be determined and the combined section used in a relatively simple arch analysis of the rib structure."

~~shell has to carry additional forces. By determining the "effective width" of the shell, the simple "Arch Theory" can be used in designing the ribs.~~

Lateral horizontal forces, caused, for example, by the wind action on the front and back door of large span cylindrical shell roofs, (Fig.1) can reach a considerable magnitude. Their influence on the structure can no longer be neglected as secondary. A difference of temperature inside and outside of the building may produce relatively high thermal stresses. Very important become the effects of shrinkage and plastic flow on the stability of the structure. These are just a few of the additional problems to be considered in the analysis of large shell roofs.

The Roberts and Schaefer Company, on the basis of their broad experience in designing and building shell roofs, decided to sponsor a two-year research program on shell arch roofs at Fritz Engineering Laboratory, Lehigh University, Bethlehem, Pa., with special emphasis on the questions mentioned above.* A careful theoretical study of the problems was made and the results were checked experimentally on a model of a cylindrical shell roof (Fig. 10). The work resulted in a number of reports (Ref. (18)), from which in this paper 3 contributions to the analysis of shell roofs are presented. It will be shown that the model tests are in excellent agreement with the theory.

*The Project was started Jan. 1, 1949 and terminated Feb. 15, 1951.

I. Effective width of cylindrical shells reinforced by ribs in circumferential direction:*

It is well known that the stress distribution in the flange of a T-Beam with a straight axis, subjected to bending in the plane of the rib, is not constant over the width of the flange (Fig. 2). The simple "Beam Theory", based on the Navier-Bernoulli hypothesis that strain due to bending varies linearly, can be "saved" if the actual width of the flange is replaced by the effective width b. Th.v. Karman (9) was first to derive the correct theoretical expression for the effective width. (See (10) for a recent resumé of the most important articles published about this subject). Shear lag is responsible for the considerable damping of the direct stresses in the flange in direction of the rib.

Consider now a cylindrical shell stiffened by a rib in circumferential direction (Fig. 3). Arbitrary loads, acting in the plane of the rib will cause direct forces N_φ per unit width in circumferential direction as shown in this figure. The actual cylinder may be replaced by a ring of width b for which a constant direct force $(N_\varphi)_{x=0}$, equal to $(N_\varphi)_{x=0}$ of the cylinder, over the entire width is assumed. By determining the width b so that

$$\underset{\text{(Ring)}}{b(N_\varphi)_{x=0}} = \underset{\text{(Cylinder)}}{\int N_\varphi \, dx}$$

the stresses in the ribs are obviously identical for both structures under an equal load system. Once the width b, called the effective width of the cylinder, is known, the calculation of the rib stresses becomes a problem of the "Simple Beam Theory" (cross sections remain plane).

*Only a very short outline of this problem can be given here. For a complete study references (15) and (16) should be consulted.

In Item 3

"INSERT ON PAGE 5.

Riezeno and Koch[17] have derived expressions for the effective width of a shell that extends indefinitely on either side of a rib. This is a special case ($\beta l = \infty$ in Fig. 4) of the author's more general solution where the rib may be any distance "l" from a free boundary."

Fig. 4)

Analytical expressions for the effective width, based on the general bending theory of cylindrical shells (e.g. Ref. (11), p. 433), were derived in Ref. (15). Ref. (16) is a short report on this study and compares the analytical values for b with experimental results. It is shown that essentially two effects govern the effective width of cylindrical shells, (1) the lag of the direct shear forces in the plane of the shell (as in the case of a T-Beam with a straight axis) and (2) the radial escaping of the shell under the circumferential direct forces N_φ. In general b can be written (see Ref. (15), p. 41):

INSERT SEE BACK OF PAGE 4.

$$b = K\sqrt{ah} \qquad (1)$$

Where: b = effective width
a = radius of the cylinder
h = thickness of the cylinder
K = f (λ, $\beta\ell$) given in Fig. 4.

The parameter λ, used in Fig. 4, takes into account the influence of the direct shear forces on the effective width:

$$\lambda = n\sqrt{\frac{h}{a}} \qquad (2)$$

where n depends on the variation of the stresses in circumferential direction (n is the number of complete waves made by a harmonic function around the circumference of the cylinder, see Fig.4). For n=0, the stress distribution has axial symmetry (e.g. constant radial line load around the rib) and the effective width has its maximum value. The parameter $\beta\ell$ depends on the length of the overhang ℓ of the shell and on the shell constant β

$$\beta = \frac{\sqrt[4]{3}}{\sqrt{ah}} \; * \qquad (3)$$

As shown in Fig. 4, the shell is assumed to extend to infinity on

*See e.g. Ref. (11), p. 392: $\beta^4 = \frac{3(1-\nu^2)}{a^2 h^2}$. The influence on b of Poisson's ratio ν is insignificant, and hence ν is neglected in Eq. (3).

the left side. This may be safely done, if the factor $\beta d > 2.4$, where d is the distance of the end from the rib (see Ref. (15) p. 25).

Taking the effective width b as flange and the rib as web of a T-section, the Bernoulli-Navier hypothesis leads to the correct values for the rib stresses. Furthermore, calling the circumferential stress along the connecting line of rib and shell σ_A, the total direct force S in the shell is the integral of all direct forces $N_\varphi = \sigma_\varphi h$ over the entire length of the shell, or equal to the product of the stress σ_A, the thickness h and the effective width b:

$$S = \int N_\varphi dx = \sigma_A hb \qquad (4)$$

For a given S and a given set of boundary conditions all forces and moments in the shell can be calculated. Ref. (15) gives a number of tables and graphs which reduce these calculations to a minimum.

In summary, the knowledge of the effective width of a cylindrical shell simplifies a very involved problem of elasticity to a common problem of the ordinary Beam Theory. In the following chapters use of this effective width is made for the analysis of shell roofs.

II. Cylindrical Shell Roof subjected to horizontal longitudinal forces.

The action of the wind on the front and back door of cylindrical shell roofs (Fig. 1) produces considerable horizontal force. An analysis for this type of a loading is presented and numerical results are compared to test results obtained on a model.

1.) Problem:

One unit* of a cylindrical shell roof, shown in Fig. 5 is subjected to horizontal forces in the direction of the axis. On a cross section a shear force V, a bending moment M_B and a twisting moment M_T are acting. The problem is to find the stress distribution due to these forces and moments.

Consider a part of infinitesimal width $a\,d\varphi$ cut out (Fig.6). The forces and moments acting on a infinitesimal shell element $dx.a\,d\varphi$ are defined in Fig. 7. Obviously the direct force N_x in axial direction is equal to the applied uniformly distributed force p at the rib $x = 2\ell$ and equal to zero at the rib $x = 0$. Assuming a linear variation of N_x along the x - axis,** then

$$N_x = \frac{x}{2\ell}\, p \qquad (5)$$

$$\text{and} \quad \frac{\partial N_x}{\partial x} = \frac{1}{2\ell}\, p \qquad (6)$$

The equilibrium of an infinitesimal shell element $dx.a\,d\varphi$ in x - direction gives (Fig. 6)

$$\frac{\partial N_x}{\partial x}\, dx\,a\,d\varphi + \frac{\partial N_{\varphi x}}{\partial \varphi}\, d\varphi\, dx = 0$$

And replacing $\frac{\partial N_x}{\partial x}$ by its value of Eq. (6)

$$\frac{\partial N_{\varphi x}}{\partial \varphi} = -\frac{a}{2\ell}\, p \qquad (7)$$

By integrating Eq. (7) and considering the fact that the shear force $N_{x\varphi}$ is zero at the center of the span, due to symmetry conditions, $N_{\varphi x}$ becomes

$$N_{\varphi x} = -\frac{a}{2\ell}\, p\, \varphi$$

---

*The erection of cylindrical shell roofs is made in units in order to re-use the form work and furthermore to provide dilatation joints.

**This assumption holds certainly for shell roofs whose width is relatively small to the span L.

It results that $N_{\varphi x}$ is constant for a section φ = constant and varies proportional to the angle φ along the span of the shell. From the equality of the shear forces $\tau_{\varphi x} = \tau_{x\varphi}$, the direct shear forces $N_{x\varphi}$ in radial direction can be taken equal to the direct shear forces $N_{\varphi x}$ as a good approximation:*

$$N_{x\varphi} \cong N_{\varphi x} = - \frac{a}{2l} p \varphi \qquad (9)$$

If imaginary support forces $N_{x\varphi}$, acting along the outer ribs $x = 0$ and $x = 2l$, are assumed, the shell is in equilibrium under the load p and subjected to shear forces $N_{x\varphi}$ and $N_{\varphi x}$, and direct forces N_x only. Actually these imaginary forces are not acting. Introducing shear forces $-N_{x\varphi}$ acting along the connecting line of the shell and the ribs these imaginary forces $N_{x\varphi}$ are eliminated.** The interaction between the rib and the shell is taken into account by considering the effective width of the shell as a flange of the rib. This effective section, consisting of the rib and the effective width, is used in analyzing the arches.

2.) Analysis of the Ribs
(calculations for rib $x = 2l$)

The ribs are acted upon by the shear loads $N_{x\varphi}$ per unit length, acting along the connecting line of the rib and the shell, positive as shown in Fig. 8.*** The distance of the loads $N_{x\varphi}$ from the centroid of the effective section is called z_A. Statically speaking, the rib is an elastically restrained arch, having two redundants only, due to symmetry of the structure and load with respect to the center line. In Fig. 8 half of one rib is shown with horizontal thrust H_c and the bending moment M_c as redundants at the center. The two

---

*$N_{x\varphi}$ is not exactly equal to $N_{\varphi x}$ due to the curvature of the shell. See e.g. Ref. (12), P. 112, Eq. (65)

**The procedure has some similarity with the "Moment Distribution" procedure. There, the joints are locked by imaginary moments which afterwards are eliminated, by introducing them in the opposite direction.

***Positive $N_{x\varphi}$ forces are acting in the opposite sense on the rib $x = 0$; see Fig. 6 for the sign convention of the $N_{x\varphi}$ forces.

geometrical conditions furnishing the two equations for the solution of H_c and M_c are a known horizontal movement δ_K of the foundation and a known rotation ϕ_K. For a fully restrained rib the conditions are:

$$\left.\begin{aligned} \varphi = \varphi_k : \delta_K &= 0 \\ \phi_K &= 0 \end{aligned}\right\} (10)$$

In case of an elastically restrained arch, with known measured foundation movements in addition, the conditions are:

$$\left.\begin{aligned} \varphi = \varphi_K : \delta_K &= (\delta_K)_{meas} \\ \phi_K &= (\phi_K)_{meas} - \kappa M_K \end{aligned}\right\} (11) \quad (\kappa = \text{Greek Kappa})$$

$(\delta_K)_{meas}$ and $(\phi_K)_{meas}$ are the measured horizontal displacement and rotation of the abutment respectively. κ being the coefficient of elastic restraint, the product $-\kappa M_K$, where M_K is the restraining moment, represents the elastic end rotation of the rib.*

In general, the shape of the center line of the rib and the variation of the moment of inertia of the effective section require a numerical procedure for the calculation of the two redundants H_c and M_c. For the special case of a circular center line and a constant I, the calculation of H_c and M_c by direct integration is shown. Extension easily may be made to other cases, e.g. parabolic shape of the rib and $I = \frac{I_c}{\cos\varphi}$, or to a numerical solution.

For the rib shown in Fig. 8 the normal force N_o and the bending moment M_o, due to the shear load $N_x\varphi$, may be obtained by integrating the contribution of the distributed shear load. If φ is the angle at which N_o and M_o are determined, let $N_x\varphi \cdot ad\omega$ represent the shear load applied over an infinitesimal rib length $ad\omega$ at any angle ω between 0 and φ. Then: (Fig. 8b)

*Further explanation for κ (under II, 3,) p. 12.

$$N_o = -\int_0^{\varphi} N_{x\varphi}\, a \cos(\varphi-\omega)\, d\omega$$

Substituting from Eq. (9) - $N_{x\varphi} = \frac{a}{2z} p\varphi$ and performing the integration

$$N_o = -\frac{a^2 p}{2z}(1 - \cos\varphi) \qquad (12)$$

Similarly, the contribution to the moment M_o of the incremental shear load is $N_{x\varphi}\, a\, d\omega$ multiplied by the moment arm $z_a - a_e\left[1 - \cos(\varphi-\omega)\right]$, where $a_e = a + z_a$ is the radius of the effective section (Fig. 8b). The integrated total of M_o then is,

$$M_o = \int_0^{\varphi} N_{x\varphi}\, a \left[z_a - a_e\left[1 - \cos(\varphi-\omega)\right]\right] d\omega$$

Substituting as before for $-N_{x\varphi}$ and integrating,

$$M_o = \frac{a^2 a_e p}{2z}\left[\left(1 - \frac{z_A}{a_e}\right)\frac{\varphi^2}{2} - 1 + \cos\varphi\right] \qquad (13)$$

The total normal force N and the total bending moment M are hence (Fig. 8a)

$$N = N_o - H_c \cos\varphi \qquad (14)$$

$$M = M_o + H_c a_e(1-\cos\varphi) + M_c \qquad (15)$$

In order to calculate H_c and M_c the horizontal displacement δ_K and the rotation ϕ_K of the abutment must be calculated. Choosing a virtual load system as shown in Fig. 8c, P' = 1 at the abutment produces the following virtual normal force N' and virtual bending moment M' at an angle φ in the rib:

$$P' = 1 : N' = -\cos\varphi \qquad (16)$$

$$M' = -a_e(\cos\varphi - \cos\varphi_k) \qquad (17)$$

By means of the work equation the displacement δ_K of the actual system is expressed as the work done by the virtual load P' = 1* :

$$\delta_k = \int \frac{M'M\,ds}{EI} + \int \frac{N'N\,ds}{EA}$$

Where: $ds = a_e d\varphi$

The influence of the normal force N on the displacement is extremely small and therefore, disregarded. Assuming, EI is constant, and

*See any textbook about Elastic Strain ~~Engineering~~ Energy Methods

replacing M' and M by their values (17) and (15) respectively, δ_k becomes:

$$\delta_k = \frac{1}{EI}\int_0^{\varphi_k} \left[-a_e(\cos\varphi - \cos\varphi_k)\right]\left[M_o + H_c a_e(1-\cos\varphi) + M_c\right] a_e d\varphi$$

Replacing M_o by (13) and integrating gives

$$-\delta_k \frac{EI}{a_e^2} = M_c(\sin\varphi_k - \varphi_k\cos\varphi_k) + H_c a_e(\sin\varphi_k + \tfrac{1}{4}\sin 2\varphi_k - \tfrac{1}{2}\varphi_k - \varphi_k\cos\varphi_k)$$
$$+ \frac{a^2 p}{2l} a_e\left[(1-\frac{z_a}{a_e})\left(\varphi_k\cos\varphi_k + (\frac{\varphi_k^2}{2}-1)\sin\varphi_k - \frac{\varphi_k^3}{6}\cos\varphi_k\right)\right.$$
$$\left. - \sin\varphi_k - \tfrac{1}{4}\sin 2\varphi_k + \tfrac{1}{2}\varphi_k + \varphi_k\cos\varphi_k\right] \qquad (18)$$

The rotation ϕ_k of the abutment is calculated by the same procedure. The virtual moment $M'_k = 1$ of Fig. 8c produces a bending moment $M' = 1$ for any angle φ:

$$M'_k = 1: \quad M' = 1 \qquad (19)$$

Inserting in the work equation

$$\phi_k = \int \frac{M'M\,ds}{EI} \qquad , ds = a_e d\varphi$$

the expression (19) and (15), ϕ_k becomes

$$\phi_k = \frac{I}{EI}\int_0^{\varphi_k}\left[M_o + H_c a_e(1-\cos\varphi) + M_c\right] a_e d\varphi$$

If M_o is substituted by its value (15) the integration can be performed

$$\phi_k \frac{EI}{a_e} = M_c\varphi_k + H_c a_e(\varphi_k - \sin\varphi_k) + \frac{a^2 p}{2l} a_e\left[(1-\frac{z_a}{a})\frac{\varphi_k^3}{6} - \varphi_k + \sin\varphi_k\right] \qquad (20)$$

(18) and (20) are two equations with the 2 unknowns H_c and M_c. δ_k and ϕ_k are given by (10) or (11) respectively. Once the redundants are known the normal force N and the bending moment M for any angle φ are given by (14) and (15). The stresses in the ribs are determined by the usual formula for combined direct force N and the bending moment M

$$\sigma = \frac{N}{A} \pm \frac{Mz}{I} \qquad (21)$$

A and I are the cross sectional area and the moment of inertia of the effective section, consisting of the rib as a web and the effective width of the shell as a flange. z is the distance of a fiber from the centroidal axis of the effective section.

3.) Coefficient of elastic restraint k:

In Eq. (11) a coefficient of elastic restraint k was introduced. In arch bridges it takes into account the elasticity of the soil and the abutment. In general the arch can't be considered fully restrained at the springing line.

In the present case another consideration led to the introduction of k. The section A - A of Fig. 10 gives a typical construction detail at the springing line of rib and shell. The latter is supported by a relatively flexible edge-member. The rib on the other hand terminates in a very heavy end-wall and may be regarded as fully restrained. Consider the two extreme cases where (1) the shell is held rigidly along the edge-member or (2) has a free edge. In the first case the N_φ - forces of the shell will be taken by the support and the effective width is constant down to the edge-member (Fig. 9a). If there is no support at all, the effective width must reduce to zero at the springing line. (Fig.9b). The actual condition is somewhere in between. This disturbance of the effective width of the shell due to edge-member action being of very local character, the reduction of the moment of inertia of the effective section can be taken into account by considering the I as constant down to the springing line and assuming an elastic restraint for the rib. The higher flexibility of the effective section in the end zone is "concentrated" at the springing line.

It is quite obvious that the magnitude of the coefficient of elastic restraint depends on the effectiveness of the edge-member

in supporting the shell. No theoretical analysis has been made of k in the present investigation.

4.) Calculation of the Shell Forces:

The stress along the connecting line of rib and shell σ_A is calculated by means of Eq. (21), once the normal force N and the bending moment M of the effective section are known. The total circumferential direct force S of the shell is (Eq. (4)).

$$S = bh\sigma_A$$

The problem consists in finding the forces and moments in the shell for a given S and a given set of boundary conditions. In the present case the boundary conditions for the shell at the ribs $x = 0$ and $x = 2l$ are:

$$\left.\begin{matrix} x = 2l \\ x = 0 \end{matrix}\right\} : \quad \begin{matrix} M_x = 0 \\ S = \text{given} \end{matrix}$$

M_x being the bending moment of the shell in axial direction per unit width, the condition $M_x = 0$ presupposes the neglecting of the torsional stiffness of the rib. The influence of the boundaries $x = l$ (middle rib) on the stress distribution can be disregarded, the forces and moments being rapidly damped out with increasing distance from the ribs $x = 0$ and $x = 2l$. Actual calculations may be found in reference (18), 213-C.

5.) Deflections of the rib:

Knowing the area A and the moment of inertia I of the effective section, the normal force N and the bending moment M for any angle φ along the rib, the deflection of the rib is readily determined by the work equation. Putting a dummy load $P' = 1$ at the point for which the deflection is desired, the work of this unit load due to the deformations caused by the actual load system, is equal to the deflection under consideration, or

$$\delta = \int \frac{M'Mds}{EI} + \int \frac{N'Nds}{EA}$$

where N' and M' are due to P' = 1, and M and N due to the actual load system.

6.) Numerical Example:

The foregoing theory is now applied to the analytical solution of a model of a shell roof construction. Fig. 10 gives the dimensions of the model approximately 1/30 of that of the actual structure (e.g. hangar at Rapid City, S.D.). Structural steel was chosen as material for the model, the dimensions (shell thickness about 1/8") leaving practically no other choice. The following list gives the principal dimensions and properties:

List:

Outer ribs:	Height	$r = 2.113"$
	Thickness	$t = 0.505"$
	Angle	$\varphi_k = 0.5866$ radians
Middle rib: (Used later on)	Height	$r = 2.113"$
	Thickness	$t = 0.625"$
Shell:	Radius	$a = 108"$
	Thickness	$h = 0.118"$
	Distance l	$l = 12"$
Load: *		$p = 140.62$ lb/in

Measured support movements:

(1) Rib $x = 2l$: $\delta_k = 1.03 \cdot 10^{-2}$ in; $\phi_k = -1.074 \cdot 10^{-3}$ radians

(2) Rib $x = 0$: $\delta_k = -1.03 \cdot 10^{-2}$ in; $\phi_k = 1.074 \cdot 10^{-3}$ radians

Material constant (E-Modulus): $E = 30 \cdot 10^6$ lb/in^2

Coefficient of elastic restraint: $k = 0.2 \frac{a_e}{EI}$

Effective Section of the Outer Ribs:

First, the effective width of the shell is calculated. Fig.4 gives a chart of the effective width under general conditions. The

*See p. ~~18~~ 17 and Fig. ~~5~~ 5 where the actual loading condition is described.

coefficient

$$\beta = \frac{1.3161}{\sqrt{ah}} = 0.3687$$

To know the number n, the stress distribution along the rib in circumferential direction has to be known. Anticipating the final results, Fig. 12 shows the stress in the ribs. The stress σ_L (σ_A has the same variation) in the lower fiber has approximately the form of a cosine-function, with a half-wave length of $\phi = 0.35$ to 0.40 radians. The number n becomes

$$n = \frac{\pi}{\text{half-wave length}} \cong \frac{3\pi}{2\varphi_k}$$

The right side of this equation is an approximate expression for n in terms of the angle of opening φ_k and holds for this particular load case only, for another load would produce another variation of the stress σ_L. Substituting the numerical value for φ_k,

$$n = 8.03$$

And the coefficient λ is

$$\lambda = n\sqrt{\frac{h}{a}} = 0.26$$

The two outer ribs have no overhang (length of overhang $l = 0$) and the distance to the middle rib ($l = 12$ in) is sufficiently large to be considered as infinitely long

($\beta l = 0.3687 \times 12 = 4.42 > 2.4$; see p. 6)

Entering the chart of Fig. 4 one may read out the coefficient K:

$$\left.\begin{array}{l} \text{For: } \beta l = 0 \\ \qquad \lambda = 0.26 \end{array}\right\} \quad K = 0.38$$

It may be seen, that up to $\lambda = 0.75$ the coefficient K and the effective width stay practically constant.

The effective width b becomes

$$b = K\sqrt{ah} = 1.36 \text{ in}$$

The area A and the moment of inertia I of the effective section are calculated next. Fig. 11a gives all pertinent information:

Area $A = 1.227 \text{ in}^2$

Distances z $z_u = 1.186$ in

$z_L = 0.926$ in

$z_a = 0.867$ in

Radius of effective section $a_e = 108.926$ in.

Moment of Inertia $I = 0.536 \text{ in}^4$

A comparison to the moment of inertia of the rib only is interesting

$$\text{Ratio } \frac{I \text{ (effective section)}}{I \text{ (rib only)}} = \frac{0.536}{0.397} = 1.35$$

It should be noted that the shell increases the bending stiffness of the rib by 35%.

The shear loads $N_{x\varphi}$ acting on the ribs are determined from Eq. (9).

$$N_{x\varphi} = - \frac{a\, p}{2} \varphi = - 632.8\, \varphi$$

All values are now available to solve the two equations (18) and (20) for the two redundants H_c and M_c. The solution is made for the assumption of a rigid restraint (conditions (10)) and an elastic restraint with measured displacement and rotation of the foundation (conditions (11)). Eventually the following values are found

a.) Rigid restraint: $H_c = -1068$ lb

$M_c = + 3156$ in - lb

b.) Elastic restraint: $H_c = -1457$ lb

$M_c = + 4371$ in - lb

On the basis of these redundants the direct stresses in the ribs were worked out and are presented in Fig. 12.

88
44

132
274
81

487

The calculation of the direct forces N_φ and the cross bending moment M_x in the shell followed the procedure briefly outlined on p. 13. The results are presented in Fig. 13.

7.) Experimental investigation and comparison

An extensive experimental study on the model, shown in Fig. 10 and 15 was made, 44 rosette (type AR-1), 137 cross (AX-5) and 81 single (A-5) SR-4 electrical strain gages recorded strains, about 20 Ames Dial gages measured displacements (accuracy 0.001 in), and two level bars checked rotations (accuracy 0.0002 rad.). The actual loading consisted of 10 equally spaced horizontal single loads as shown in Fig. 5b. By virtue of St. Venant's principle the differences between the theoretical loading, assumed uniformly distributed, and the actual loading can cause only local differences in behavior.

The stresses in the ribs computed from the strain gage readings are shown in Fig. 12. Note the agreement between test and theory if the analysis is made with arbitrary allowance for the elastic restraint of the rib. The introduction of k is fully justified. In Fig. 13 the experimental N_φ (direct force per unit width of the shell in circumferential direction) and M_x (bending moment per unit width in axial direction) of the shell are plotted.

The correspondence between the analytical and theoretical results is quite close. It is interesting to note that the stress distribution is perfectly antisymmetric with respect to the middle rib. The latter is unstressed, therefore contributes nothing to the strength of the structure under the present type of a loading. The rib $x = 2l$ has exactly the opposite stresses of the rib $x = 0$. This fact is also demonstrated in Fig. 14 where the measured vertical deflections of both outer ribs are plotted. For the center $\varphi = 0$ the calculated deflections are also shown.

8.) Conclusions:

1. The analysis of the effect of horizontal lateral wind loads on cylindrical shell roofs, developed in this chapter, was fully confirmed by an experimental investigation on a model.

2. For actual shell roofs of the Rapid City type (span 340 ft.), the wind pressure on the front door (as prescribed by building codes) is 30 to 35 lb/ft^2, or approximately 1000 lb/ft of the rib. This results in maximum rib stresses of about 400 lb/in^2. Obviously, a stress of this magnitude cannot be disregarded as a secondary one. By combining a number of units these stresses can be lowered considerably.

III Foundation Movements:

1.) The Problem:

The horizontal thrusts of modern long span shell roofs are large enough to offer serious foundation problems. In certain cases, tension ties have been found necessary to balance the horizontal thrust acting on the abutments. (Ref. (7), p. 35). In any case, it usually will be impossible to prevent completely any foundation movements, except by very special devices, as for example artificial stressing of tension ties between the abutments. The importance of an analysis for the foundation movements is therefore obvious.

The general procedure for the calculation of arches subjected to foundation movements may be used if the interaction, occurring between the ribs and the shell, is taken into account. This will be done as in the previous chapter by taking as cross section of the rib the effective cross section formed by the rib and the effective width of the shell.

2.) Analysis of the ribs:

A horizontal displacement δ_k and symmetrical rotations ϕ_k of the two abutments are considered. Unequal rotations $\phi_{k\ell}$ and ϕ_{kr} of the left and the right abutments can be solved by superimposing symmetrical rotations $\phi_k = \frac{1}{2}(\phi_{k\ell} + \phi_{kr})$ and anti-symmetrical rotations $\phi_k = \pm \frac{1}{2}(\phi_{k\ell} - \phi_{kr})$. The advantage of this procedure is to reduce the number of redundants from three to two.

The rib, shown in Fig. 16a, has two redundants, the horizontal thrust H_k and the end moment M_k. Introducing the virtual load $H'_k = 1$ (Fig. 16b) and the virtual moment $M'_k = 1$ (Fig. 16b), the horizontal displacement δ_k and the end rotation ϕ_k respectively can be calculated by means of the work equation.

The actual normal force N and bending moment M are (see Fig. 16a):

$$N = -H_c \cos\varphi \qquad (22)$$

$$M = M_k - H_k a_e (\cos\varphi - \cos\varphi_k) \qquad (23)$$

Due to $H'_k = 1$ (Fig. 16b)

$$N' = -\cos\varphi \qquad (24)$$

$$M' = -a_e (\cos\varphi - \cos\varphi_k) \qquad (25)$$

Hence the δ_k becomes

$$\delta_k = \int_{-\varphi_k}^{+\varphi_k} \frac{M'Mds}{EI} + \int_{-\varphi_k}^{+\varphi_k} \frac{N'Nds}{EA}$$

Assuming EI and EA constant, inserting (22), (23) and (24), (25) and performing the integration

$$\frac{EI}{2a_e^2}\delta_k = M_k(\varphi_k\cos\varphi_k - \sin\varphi_k) + H_k a_e\left[\varphi_k\left(\tfrac{1}{2} + \cos^2\varphi_k\right) - 3/4\,\sin 2\varphi_k + \frac{I}{AR^2_e}\left(\tfrac{1}{2}\varphi_k + \tfrac{1}{4}\sin 2\varphi_k\right)\right] \qquad (26)$$

Taking $M'_k = 1$ and

$$N' = 0 \qquad (27)$$

$$M' = 1 \qquad (28)$$

the work equation provides the end rotation ϕ_k. Taking into account the reduction of the effective width in the edge-member zone by a coefficient of elastic restraint κ*, the external moment $M'_k = 1$ of the virtual load system times the rotation $-\kappa M_k$ due to elastic restraint in the actual load system contribute to the external work:

$$\phi_k - \kappa M_k = \int_0^{\varphi_k} \frac{M'Mds}{EI} + \int_0^{\varphi_k} \frac{N'Nds}{EA}$$

Making the necessary substitutions by (22), (23) and (27), (28) the integration gives eventually:

$$\frac{EI}{a_e}\phi_k = M_k(\varphi_k + \bar{\kappa}) + H_k a_e(\varphi_k \cos\varphi_k - \sin\varphi_k) \qquad (29)$$

Where: $\bar{\kappa} = \frac{EI}{a_e}\kappa$

For any given values of φ_k and ϕ_k, the two redundants H_k and M_k are determined by Eq. (26) and (29). The direct stresses in the ribs are calculated by use of Eq. (21).

3.) Calculation of the Shell Forces:

The procedure is the same as described on p. 13. For the two outer ribs and the middle rib the corresponding S-Forces are calculated by Eq.(4), once the stress σ_A along the connecting line of rib and shell is known (Eq. (21)). Knowing the boundary conditions for the shell, which are

Rib $x = 0$
Rib $x = 2l$ $\Big\}$ $M_x = 0$

Rib $x = l$ $\quad \frac{\partial w}{\partial x} = 0,$

*See p. 12 for further explanation.

and the S-Forces, the stress distribution in the shell can be calculated. The presentation of this analysis, exceeding the scope of the present paper, may be found in reference (15).

4.) Numerical Example:

The model (Fig. 10) is analyzed for a given horizontal displacement δ_k and end rotation ϕ_k. The effective width of the ribs must be calculated first. In order to know the number n, used in the chart for the effective width (Fig. 4) the stress distribution along the rib must be known. Fig. ~~18~~ 17 shows that as a first approximation the variation of the stress σ_L in the lower fiber of the middle and outer ribs is a cosine function with a half-wave length $\varphi \cong 0.75$. Hence

$$n = \frac{\pi}{0.75} \cong \frac{3\pi}{4\varphi_k}$$

$\frac{3\pi}{4\varphi_k}$ is a first approximation for n if foundation movements are considered. (Note the difference to n in the case of horizontal lateral loads, p. 15.) Inserting the value of $\varphi_k = 0.5866$

$$n = 4.14$$

$$\lambda = n\sqrt{\frac{h}{a}} = 0.14$$

The coefficient β_l for the middle and outer ribs (β being computed on p. 15) are

Middle rib: $\beta_l = 0.3687 \times 12 = 4.42 > 2.4$

Outer ribs: $\beta_l = 0.3687 \times 0 = 0$

From Fig. 4 it is obvious that the values of K for (1) $\lambda = 0, \beta_l = \infty$ in case of the middle rib, and (2) $\lambda = 0, \beta_l = 0$ in case of the outer ribs are sufficiently accurate for the determination of the effective width:

(1) Middle rib: $\lambda = 0$, $\beta_l = \infty$ } $K = 1.52$

$$b = K\sqrt{ah} = 5.43 \text{ in}$$

(2) Outer rib: $\beta l = 0$, $\lambda = 0$ $\Big\}$ $K = 0.38$

$$b = K\sqrt{ah} = 1.36 \text{ in}$$

The following values for the effective section are eventually derived (compare Fig. 11a and 11b)

Middle rib:

Area		$A = 1.961 \text{ in}^2$
Distances	z	$z_M = -1.382$ in
		$z_L = 0.731$ in
		$z_A = 0.672$ in
Radius of effective section		$a_e = 108.731$ in
Moment of inertia		$I = 0.921 \text{ in}^4$

Ratio $\frac{I \text{ (effective section)}}{I \text{ (rib only)}} = \frac{0.920}{0.491} = 1.84$

Outer Ribs: (as on p. 16)

Area		$A = 1.227 \text{ in}^2$
Distances	z	$z_M = -1.186$ in
		$z_L = 0.926$ in
		$z_A = 0.867$ in
Radius of effective section		$a_e = 108.926$ in
Moment of inertia		$I = 0.536 \text{ in}^4$

Note especially the considerable increase (84%) of the bending stiffness of the middle rib by the effective width of the shell.

On the model the following horiztonal displacement δ_k and end rotation ϕ_k were induced:

$$\delta_k = -0.3300 \text{ in}$$

$$\phi_k = 7.753 \times 10^{-4} \text{ radians}$$

Taking the coefficient of elastic restraint

$$k = 0.05 \frac{a_e}{EI}$$ *

and inserting in Eq. (26) and (29) the proper values, the horizontal thrust H_k and the end moment M_k are calculated:

Middle Rib: $H_k = -1636$ lb

$M_k = -17850$ in-lb

Outer Rib: $H_k = -946$ lb

$M_k = -10350$ in-lb

Normal force N and bending moment M for an arbitrary angle φ along the rib are given by Eq. (22) and (23). The calculated rib stresses (Eq. (21)) are plotted in Fig. 17 for the middle and outer ribs.

Fig. 18 presents the normal force in a circumferential direction N_φ and the bending moment in axial direction M_x of the shell, the calculation of which was briefly outlined in III,3.

5.) Experimental investigation and comparison

The same model (Fig.10), as used for the test of lateral horizontal loads, was subjected to a horizontal foundation displacement (Fig. 19). The measured displacement and end rotations are given on p. 24.

The stresses in the ribs and the N_φ-force and M_x-moment, computed on the basis of the SR-4 strain gage readings are plotted in Fig. 17 and 18 respectively. Theory and test again compare very favorably. The discrepancy of a few experimental M_x- values in Fig. 19 does not influence the overall agreement.

---

* Note that k depends on the type of loading, for the case of horizontal lateral loads a different value for k was used (p. ~~15~~ 14).

6.) Conclusions:

1. By taking the effective width of the shell as flange of a T-section the web of which is the rib (effective section), the analysis of the ribs for foundation movements can be done by simple arch theory. Once the stresses in the ribs are known, the stress distribution in the shell can be computed also. Experimental results on the model support the proposed analysis.

2. Eq. (26) and (29) show immediately that for given foundation movements δ_k and ϕ_k, the moment M_k and the horizontal thrust H_k are proportional to the moment of inertia I of the effective section of the rib. Neglecting the influence of the normal force on the deformations, which is completely negligible one may write:

$$\left.\begin{aligned} N &= c_1(\varphi)\, I \\ M &= c_2(\varphi)\, I \end{aligned}\right\} \quad (30)$$

where: $c_1(\varphi)$, $c_2(\varphi)$ are functions depending on the angle φ only.

And the stress σ in the rib becomes (Eq. (21))

$$\sigma = \frac{c_1 I}{A} \pm \frac{c_2 I z}{I} = \frac{c_1 I}{A} \pm c_2 z \qquad (31)$$

Roughly, σ is proportional to the distance z of the fiber from the centroidal axis of the cross section, for the first term of the right side of (31) is always relatively small. The importance of these ~~deviations~~ derivations will become apparent in a later discussion (p. ~~29~~ 27).

IV SOME SPECIAL PROBLEMS:

1.) Uniform Temperature Change and Shrinkage of the Concrete:

Suppose a shell roof undergoes a uniform temperature change of Δt°. If the whole structure would be supported as a simple

beam, this temperature change would cause an increase ΔL of the span L:

$$\Delta L = \alpha \Delta t^{\circ} L$$

Where: α = coefficient of thermal expansion.

Actually this increase ΔL is impossible, for the abutments are restrained. Therefore the original span L must be restored by diminishing the new span $(L + \Delta L)$ by ΔL. The latter is exactly the horizontal displacement δ_k already treated under III. Be replacing in Eq. (26) and (29).

$$\left.\begin{aligned} \delta_k &= \alpha \Delta t^{\circ} L \\ \phi_k &= 0 \end{aligned}\right\} \quad (32)$$

the horizontal thrust H_k and the end moment M_k due to a temperature rise Δt° are thus determined.

It is common practice to consider the effect of shrinkage of the concrete as equivalent to a fall in temperature of a specified Δt°. Hence, the stress due to shrinkage may also be determined by the same procedure.

2.) Differential Temperature Change Between Ribs and Shell:

Assume a temperature difference between the outside and inside air of a shell roof structure. The ribs, exposed mostly to the outside air will have a different mean - temperature than the shell. The difference in temperature between the shell and the rib may be Δt°. Obviously stresses in the structure will be produced.

An analysis of this load case resulted in thermal stresses up to 100 lb/in^2 for a temperature difference of $10^{\circ}F$ in a hangar of the Rapid City type (340 ft. span).

The actual temperature distribution will be somewhat different from the assumed one, for the temperature will vary

continuously. Temperature measurements on an actual structure should be made to determine the variation.

3.) Stability of the Structure:

The thickness h of the shell is mainly governed by stability considerations. For a certain spacing ℓ of the ribs, a radius "a" of the shell, and a given distributed load, a minimum thickness h of the shell is required.* The resulting membrane stresses reach only a fraction of the allowable concrete stresses in compression. It may be of interest to point out that the ratio of thickness to radius of modern shell roofs is smaller than the corresponding ratio for an egg shell. This fact illustrates the perfection to which these structures have been developed.

The ribs, reinforcing the shell at regular intervals ℓ, increase the buckling stiffness of the shell panel in between. Furthermore, they are indispensible for carrying a one-sided live load (snow), acting on the structure. To provide a sufficient buckling safety for the entire structure the ribs must have a certain minimum stiffness. The buckling load is proportional to the moment of inertia of the effective section (rib plus effective width of the shell). Previous considerations concerning the stresses due to volume change led to a stiffness of the rib as small as possible. Obviously the stiffness should be kept at the minimum required for stability and bending strength so that the stresses due to volume change do not become too excessive.

Consequently, the question of the factor of safety against buckling of the ribs is of prime importance. A smaller factor of

* See Ref. (11) or (12).

safety will require less stiffness and therefore smaller stresses will be set up by volume changes. Plastic flow of the concrete affects the geometrical shape of the structure, hence the forces, in a dangerous manner, if the factor of safety is decreased too much. In addition, the secondary moments due to deformations of the structure can be correlated to the factor of safety against buckling (Ref. 13). The scope of the present investigation does not permit specific recommendations for this factor of safety but it is a very important consideration in design.

4.) Location of the shell with respect to the rib:

Recently the idea of locating the shell in the middle of the rib was brought forward (Ref. 14). Considering the stresses due to volume change Whitney correctly concluded that the stiffness of the ribs should be a minimum. By locating the shell in the middle of the rib the stiffness of the effective section is indeed diminished to a great extent (see for example below, ~~p. 41~~, 47%). But the same decrease can be obtained by taking a smaller rib, with the shell at one edge of the rib.

To illustrate, consider the following cross sections:

Section (1)

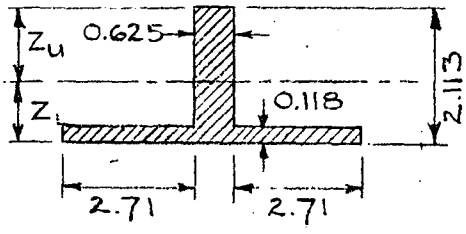

Area $A_1 = 1.9608$

Mom.I $I_1 = 0.9204$

Dist.: $z_{u1} = 1.382$

$z_{L1} = 0.731$

Section (2)

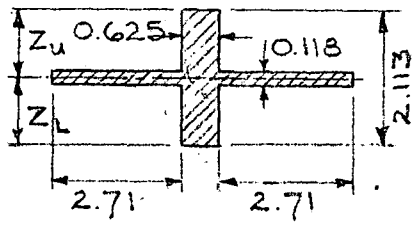

$A_2 = 1.9608$

$I_2 = 0.4914$

$z_{u2} = 1.056$

$z_{L2} = 1.056$

Section (3)

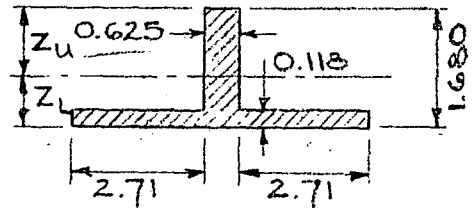

$A_3 = 1.6902$

$I_3 = 0.4895$

$z_{u3} = 1.136$

$z_{L3} = 0.544$

Sections (1) and (2) are identical, except for the location

of the rib. Placing the shell in the middle of the rib reduces the moment of inertia by 47%. Section (3) has a moment of inertia practically equal to section (2) due to a reduction in the height of the rib. The normal force and bending moment due to volume changes are proportional to the moment of inertia of the effective section (compare Eq. (26), (29) and (30)). The fiber stresses on the other hand are additionally proportional to the distance z of the fiber from the neutral axis (Eq. (31)). The ratio of the corresponding stresses of the two sections is hence equal to the ratio of the corresponding distances z:

$$\text{Upper fiber:} \quad \frac{\sigma_{u3}}{\sigma_{u2}} = \frac{z_{u3}}{z_{u2}} = \frac{1.136}{1.056} = \frac{1.08}{}$$

$$\text{Lower fiber:} \quad \frac{\sigma_{L3}}{\sigma_{L2}} =^{*} \frac{z_{L3}}{z_{L2}} = \frac{0.544}{1.056} = \frac{0.52}{}$$

Section (3) has in the upper fiber a stress 8% higher and in the lower fiber a stress 48% lower than section (2). The objection that in section (3) important cross bending stresses σ_x are set up can be rejected, for in the most extreme case σ_x is 1.73 times the lower fiber stress of the rib*:

$$\frac{\sigma_x}{\sigma_{L_2}} = 1.73 \times 0.52 = 0.90$$

The cross bending stress σ_x is still 10% smaller than σ_{L2} and furthermore, the cross bending is concentrated on a very short length.

In summary, for section (3) with a 21% lighter rib than section (2) the bending moment and normal force due to volume changes are identical. Neglecting the influence of the normal force the stresses of the section (3) are + 8% and - 48% of the ones of section (2). Cross bending stresses σ_x are - 10% and 10% lower than the maximum stress in section (2) and

*See Ref. (15), p. 42.

of local importance (σ_x has the form of a strongly damped oscillation starting from the rib). Therefore, from a statical point of view section (2) does not have any advantage over section (3) whatsoever. Contrarily, 21% of the dead weight of the rib can be saved by using section (3). It must be concluded that it is not only ineffective but wasteful to place the shell at the center of the web.

SUMMARY AND CONCLUSIONS:

Theoretical solutions for some problems encountered in designing long span cylindrical shell roofs were presented. Tests on a steel model in the scale 1 to 30 of an actual structure built in reinforced concrete (hanger Rapid City, S.D.) confirmed the theoretical results. Possible objection that the test results were obtained from a perfectly elastic structure (only elastic strains were induced in the model) whereas the material (reinforced concrete) in an actual structure exhibits quite different properties may be answered as follows:

It is common practice to calculate the forces and moments in statically indeterminate concrete structures by assuming the concrete as a perfectly elastic material. The moment of inertia for a cross section is taken for the uncracked concrete section (e.g. continuous T-Beam girders, flange in tension over the supports etc.). On the basis of the calculated moments and normal forces the stresses in the concrete and the reinforcing steel are determined under the assumption that the concrete is ineffective in tension (cracked tension zone). This may be done by using either the usual n-Theory or the so-called "limit design" Theory.

Therefore, the similitude between the theoretical direct forces and bending moments of the steel model and the concrete structure can be made (both materials are assumed to be perfectly elastic). These values were checked by test results of the model, built of a nearly perfectly elastic material. Between the stresses in the model and in the actual structure no such direct relations can be derived. But it is a well established fact, proved by many tests, that reinforced concrete structures, analyzed as elastic structures and reinforced according to the calculated moments and normal forces, behave essentially as predicted.

Many tests not reported herein were made during the course of the investigation but space does not permit their inclusion. Similar procedures of analysis, based on the use of the "effective width", were found adequate to check test results to a close approximation in all cases. It was found adequate to roughly estimate the value of "n", since the effective width for the proportions of structures tested and type of stress variation induced by usual loads put "n" in a region where variations caused little or no change in the effective width. Other engineering uncertainties are of much greater magnitude. In other applications of this report to different problems, it might be found necessary to carry out analyses by means of a Fourier Series representation of the stress variation along the juncture of the rib and shell. In such cases effective widths and stresses could be determine for each of the significant terms of the Fourier Series, and the actual stress at any point could be determined by superposition.

ACKNOWLEDGMENT

The report presents a part of the theoretical studies made during the course of a two-year research program on shell arch roofs carried out at Fritz Engineering Laboratory, Department of Civil Engineering and Mechanics, Lehigh University, Bethlehem, Pennsylvania. Professor William J. Eney is Head of the Department and Director of the Laboratory. Mr. Lynn S. Beedle, Assistant to the Director, and Mr. Kenneth R. Harpel, Laboratory Foreman, gave valuable assistance throughout the investigation.

Roberts and Schaefer Company, Chicago, Illinois, was sponsor of the research program. Many thanks are expressed to Mr. J.E. Kalinka, Executive Vice-President of the Company, and to Mr. Robert Zaborowski, Manager of the New York Office, who was representing the Company, for their continued assistance. The many suggestions received from Mr. A. Tedesko, O. Gruenwald, W. A. Renner and P. Rongved, all of Roberts and Schaefer Company, during several meetings are sincerely acknowledged.

LIST OF REFERENCES

(1) Love, A.E.H. — "Elasticity", 4th edition Cambridge Univ. Press, 1927

(2) Meissner, E. — "Das Elastizitätsproblem für dünne Schalen" Phys. Zeitschrift, vol. 14, 1913, p. 343

"Über Elastizität und Festigkeit dünner Schalen" Vierteljahrsschrift der Naturforsch. Gesellschaft, Zürich, vol. 60, 1915, p. 23

(3) Bauersfeld — See: "Handbuch fur Eisenbeton-Bau, Band VI, 4th edition Wilhelm Ernst und Sohn, 1928, p. 269

(4) Finsterwalder, U. — "Die querversteiften zylindrischen Schalengewölbe mit kreissegmentförmigem Querschnitt" Ingenieur Archiv, vol. 4, 1933, p. 43.

(5) Dischinger, F. — "Die strenge Theorie der kreiszylinderschale und ihre Anwendung und die Z.D. Schalen" Beton & Eisen, vol.34, 1935.

(6) Molke, E.C., Kalinka, J.E. — "Principles of Concrete Shell Dome Design" ACI Proceedings, vol. 9 1938, p. 649

(7) Prentiss, L.W. — "Thin Concrete Arch Roof Provides 340 Ft. Clear Span for Bomber Hangar" Civil Engineering, vol. 19, no. 2, 1949, p. 34

(8) Allen, J.E. — "Construction of Long-Span Concrete Arch Hangar at Limestone Air Force Base" ACI Proceedings, vol. 21, 1950, p. 405

(9) v.Karman, Th — "Die mittragende Breite" Festschrift Aug. Föppls Springer, Berlin, 1924, p. 114

(10) Raithel, W. — "The Determination of the Effective Width of Wide-Flanged Beams" Tech. Report No. 61, Ordnance Research and Development Division, 1949

List of References, (Continued)

(11) Timoshenko, S. "Theory of Plates and Shells" McGraw-Hill, New York, 1940

(12) Flügge, W. "Statik und Dynamik der Schalen" Springer, Berlin, 1934

(13) Dischinger, F. "Untersuchungen über die Knicksicherheit, Bauing, vol. 18, 1937, p. 487
"Elastische und plastische Verformungen Bauing, vol. 20, 1939 p. 53

(14) Whitney, Ch. S. "Cost of Long-Span Concrete Shell Roofs" ACI Proceedings, vol. 21, 1950, p. 765

(15) Thürlimann, B. "The Effective Width of Circular Cylindrical Shells Reinforced by Ribs" PhD-Dissertation, Lehigh Univ., 1950

(16) Thürlimann, B. Bereuter, R. and Johnston, B.G. "The Effective Width of a Circular Cylindrical Shell Adjacent To A Circumferential Reinforcing Rib", presented at First National Congress for Applied Mechanics, 1951, Chicago, Illinois

(17) Biezeno, C.B. Koch, J.J. "The Effective Width of Cylinders periodically Stiffened by Circular rings." Proceedings Koninklijke Nederlandsche Akademie Van Weten-Schappen, Vol. XLVIII.

(18) Thürlimann, B. Johnston, B.G. Progress Reports to Roberts & Schaefer Company of Research Project 213, 1949-50

213A-"Stress Distribution and Effective Width Adjacent to Stiffeners in Cylindrical Shells" (tests)

213B-"Stress Distribution and Effective Width Adjacent to Stiffeners in Cylindrical Shells" (analysis)

213C-"Shell Arch Roof Model under Simulated End Wind Load"

List of References (Continued)

(18, cont.)

213D-"Shell Arch Roof Model under Dead Load and Half Side Live Load"

213E-"Shell Arch Roof Model under Simulated Foundation Movements"

213F-"Shell Arch Roof Model Subjected to Two Cases of a Concentrated Load"

213G-"Experimental Test Results of a Shell Arch Roof Model under Different Types of Loading"

H. H. Bleich

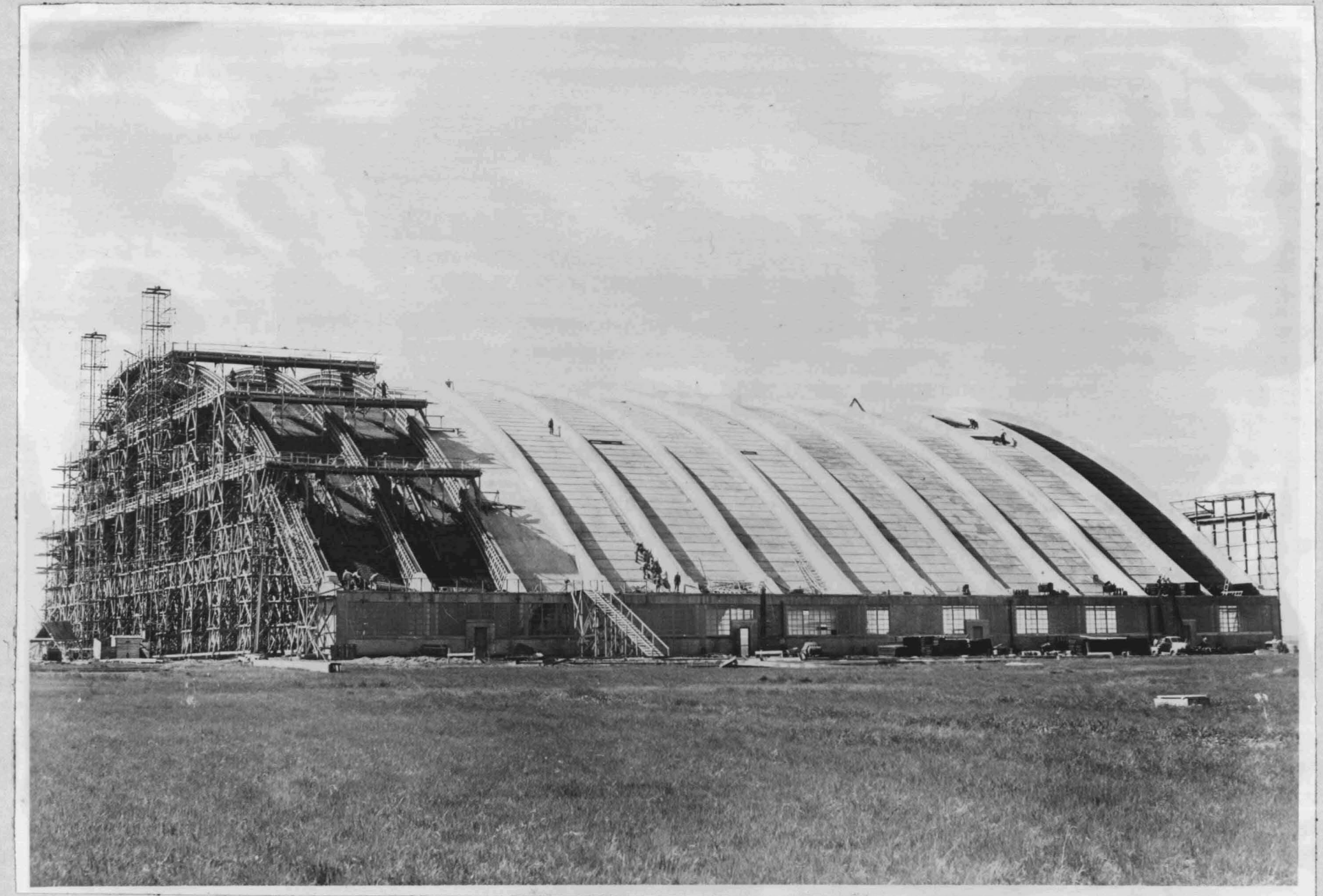

Picture of Rapid City Hangar,

showing front door and long side.

Fig. 1

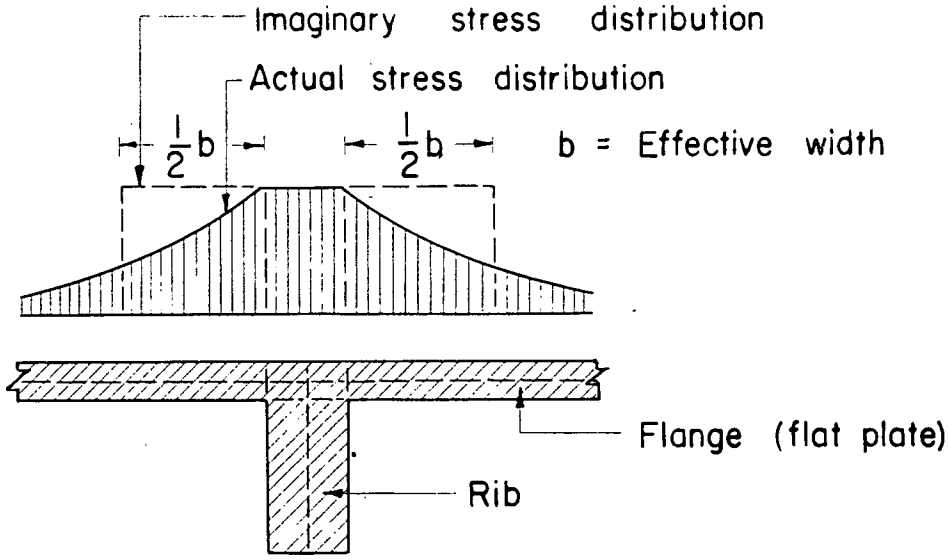

T-Beam

Fig. 2

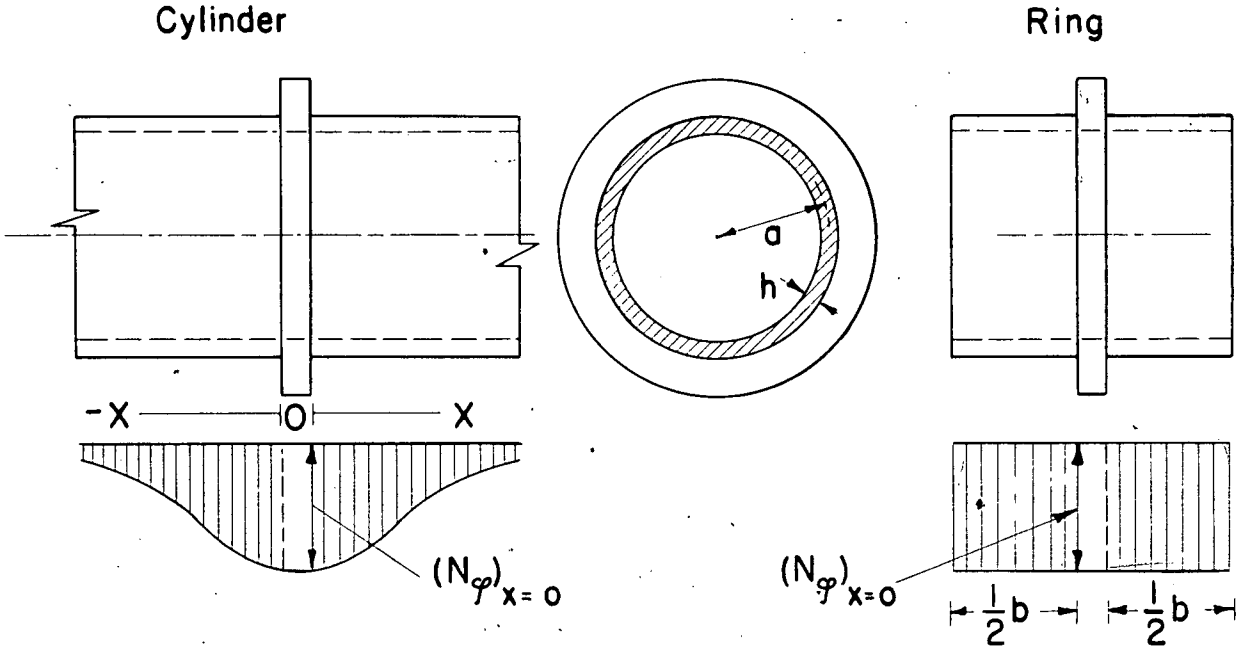

Fig. 3

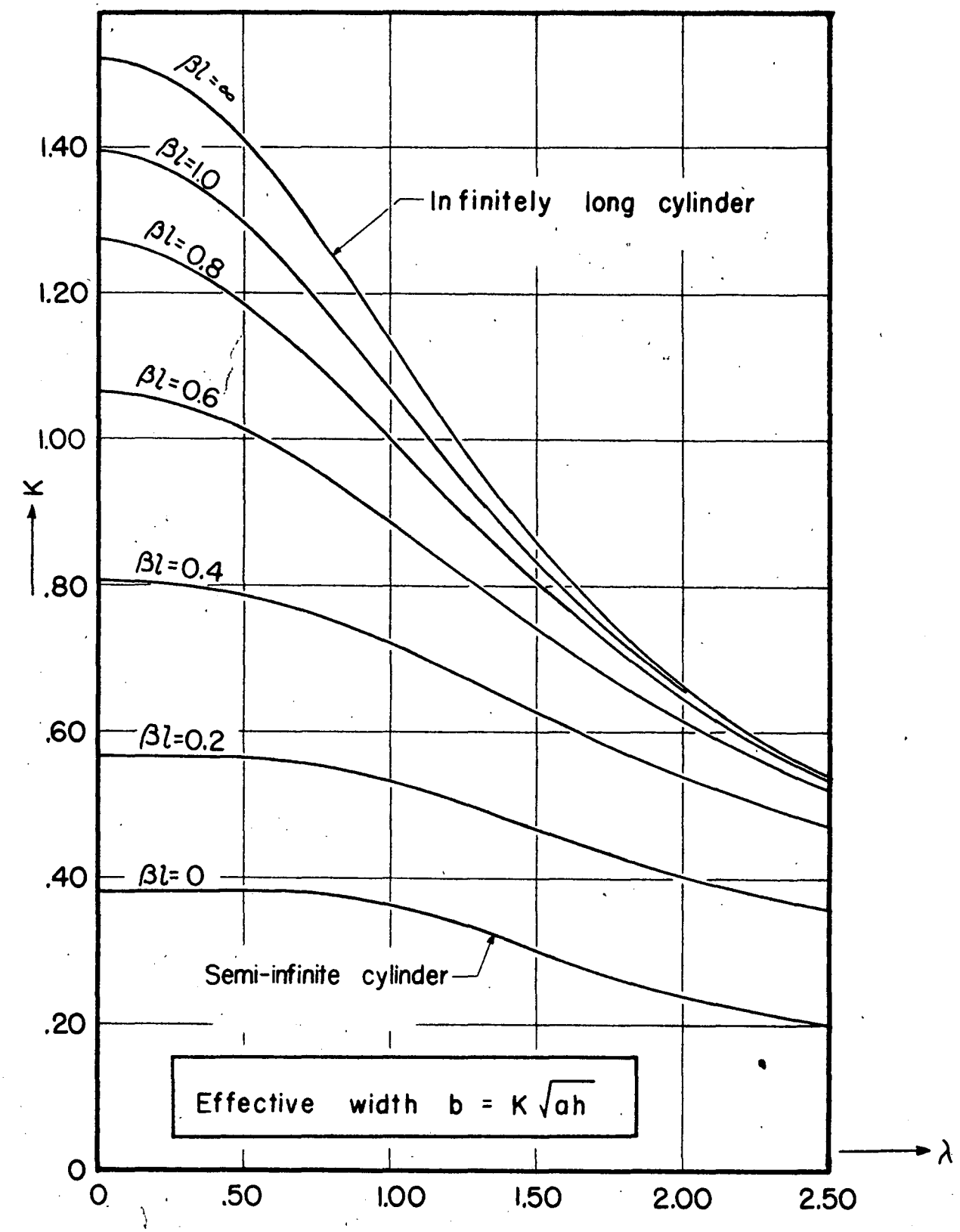

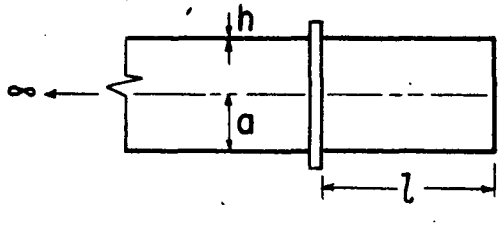

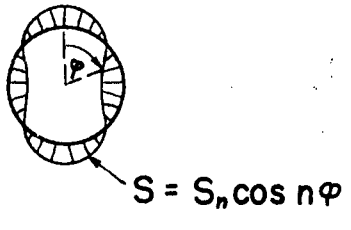

$$\lambda = n\sqrt{\frac{h}{a}}$$

$$\beta = \frac{1.3161}{\sqrt{ah}}$$

Fig. 4

a) Theoretical Loading

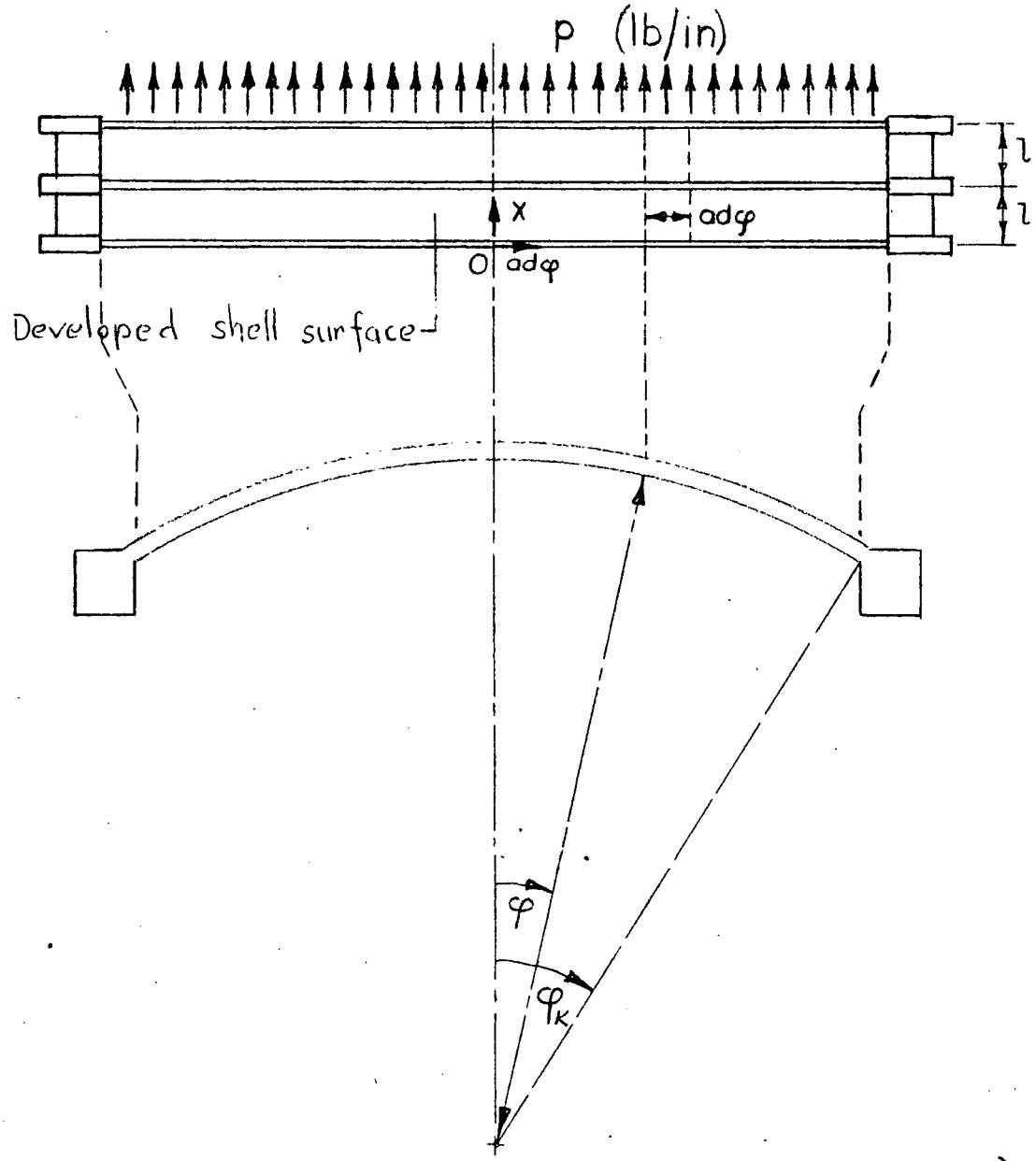

b) Actual loading in test (10 Single Loads P)

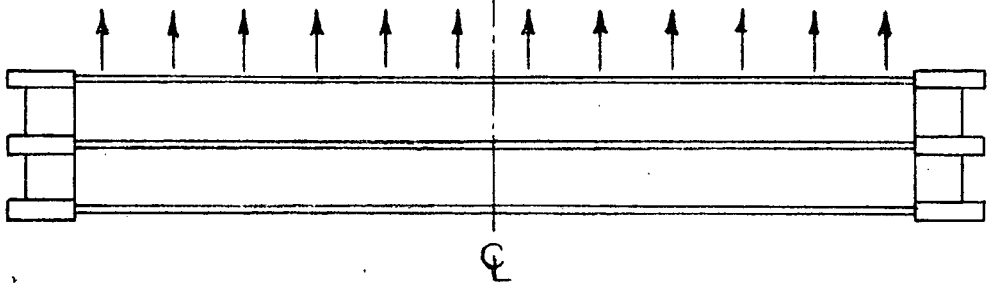

— Fig. 5 —

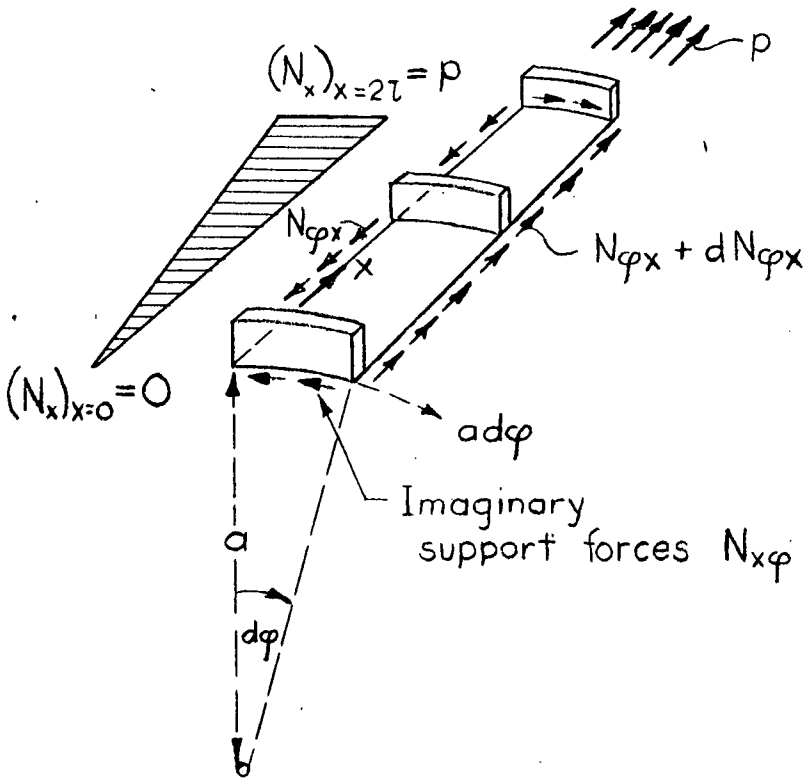
$(N_x)_{x=2l} = p$
p
$N_{\varphi x}$
x
$N_{\varphi x} + dN_{\varphi x}$
$(N_x)_{x=0} = 0$
$ad\varphi$
Imaginary
support forces $N_{x\varphi}$
a
$d\varphi$
b

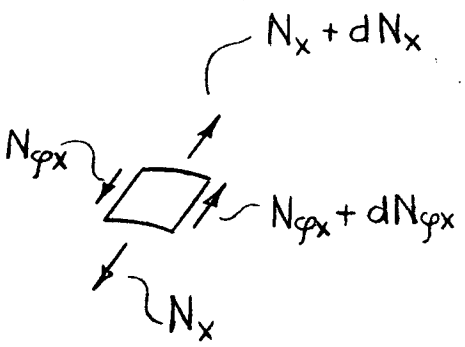
$N_x + dN_x$
$N_{\varphi x}$
$N_{\varphi x} + dN_{\varphi x}$
N_x

—Fig 6—

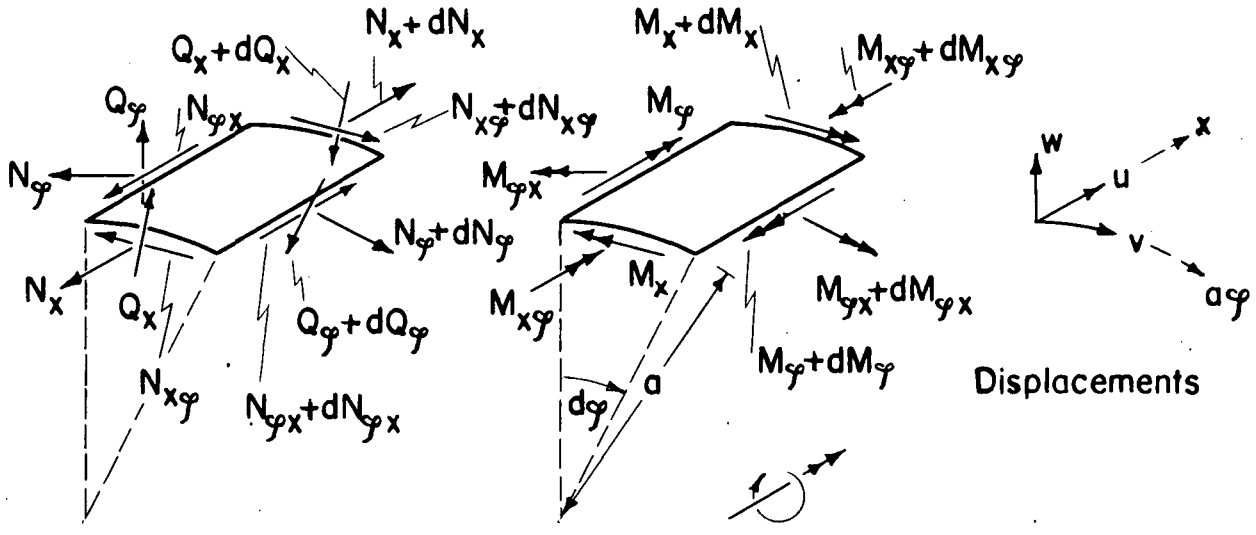
$Q_x + dQ_x$
$N_x + dN_x$
$M_x + dM_x$
$M_{x\varphi} + dM_{x\varphi}$
Q_φ
$N_{\varphi x}$
$N_{x\varphi} + dN_{x\varphi}$
M_φ
N_φ
$M_{\varphi x}$
$N_\varphi + dN_\varphi$
N_x
Q_x
$Q_\varphi + dQ_\varphi$
$M_{x\varphi}$
M_x
$M_{\varphi x} + dM_{\varphi x}$
$N_{x\varphi}$
$N_{\varphi x} + dN_{\varphi x}$
$M_\varphi + dM_\varphi$
$d\varphi$
a
w
x
u
v
a_φ
Displacements
Forces
Moments

Fig. 7

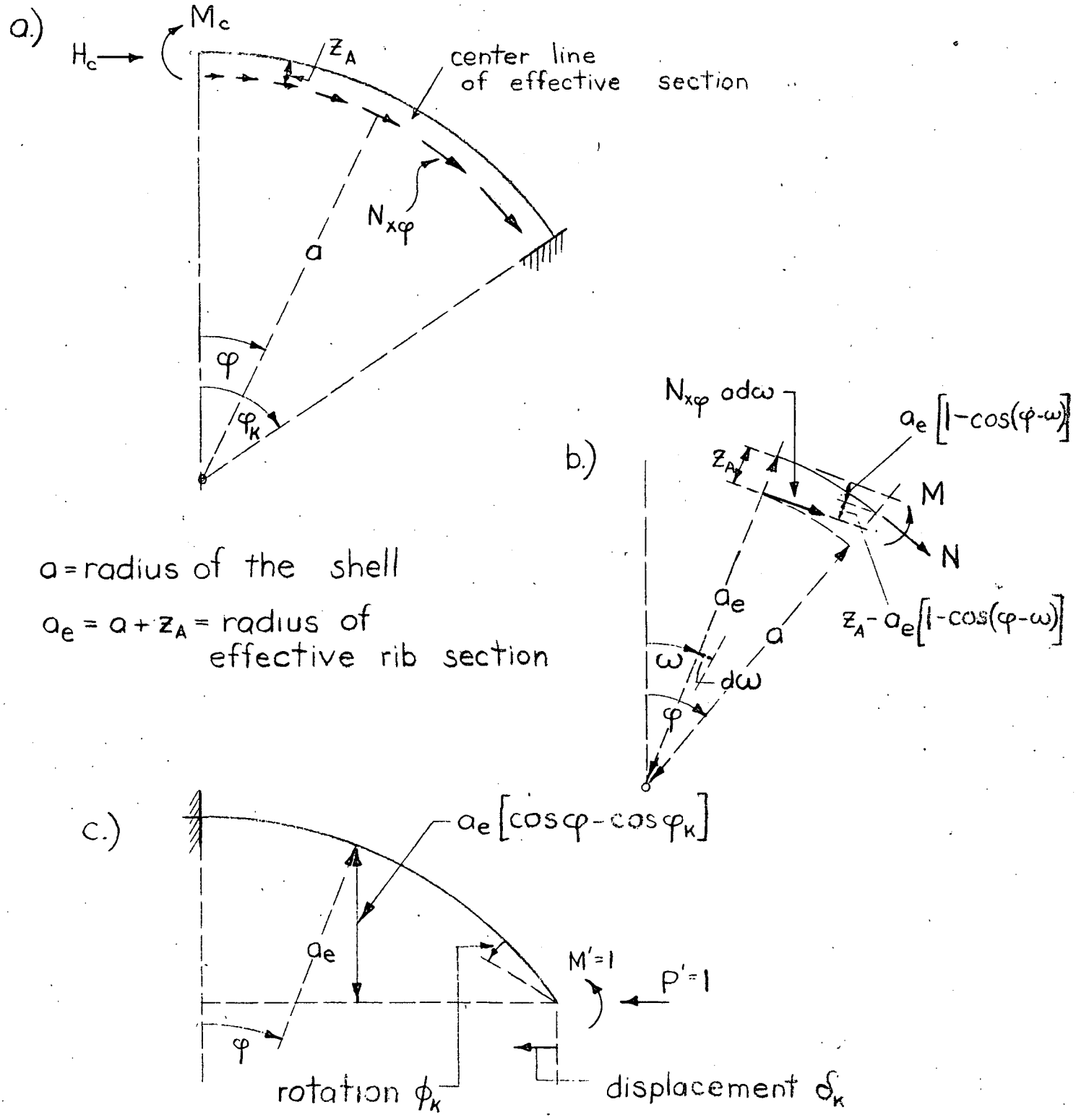

a = radius of the shell

$a_e = a + z_A$ = radius of effective rib section

—Fig. 8—

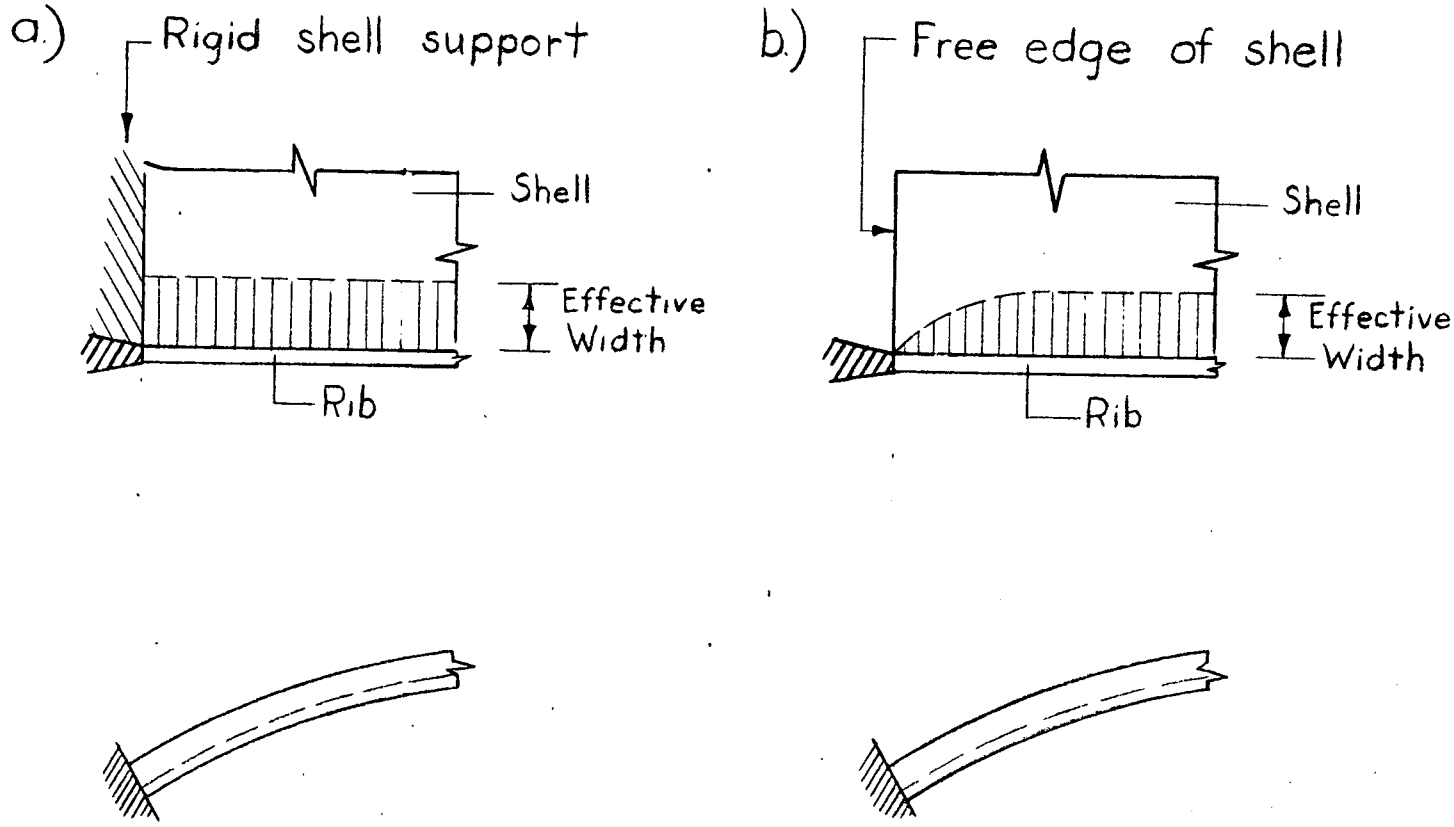
a.)
Rigid shell support
Shell
Effective Width
Rib
b.)
Free edge of shell
Shell
Effective Width
Rib

—Fig. 9—

SHELL ROOF MODEL SHOWING MEASURED DIMENSIONS.

ALL DIMENSIONS IN INCHES

FRONT VIEW 1" = 10"

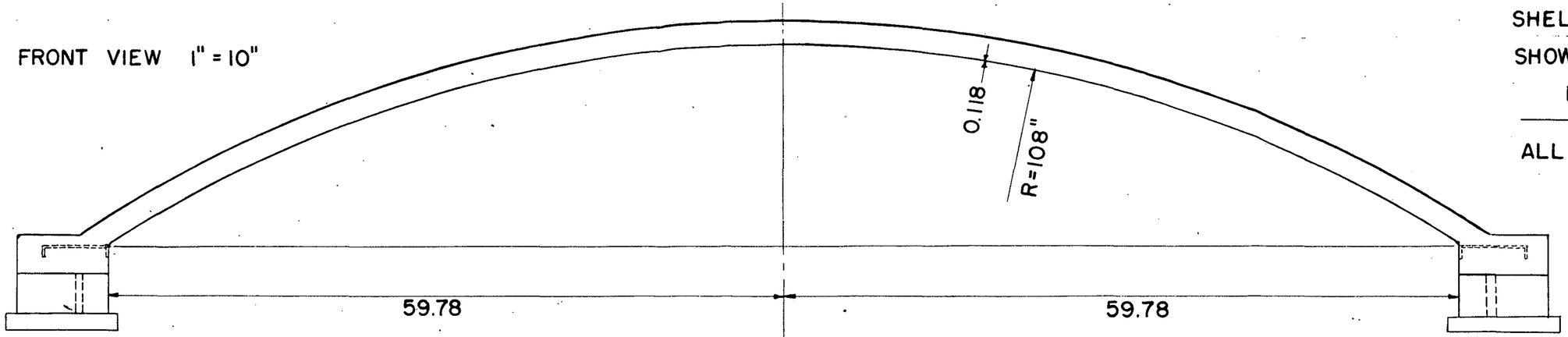

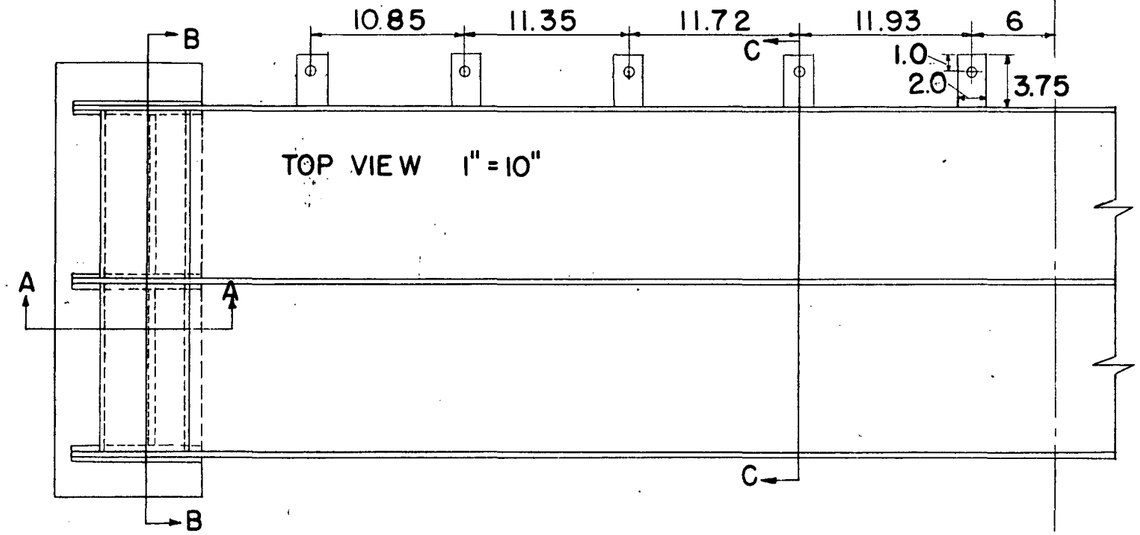

TOP VIEW 1" = 10"

SECTION C-C 1" = 4"

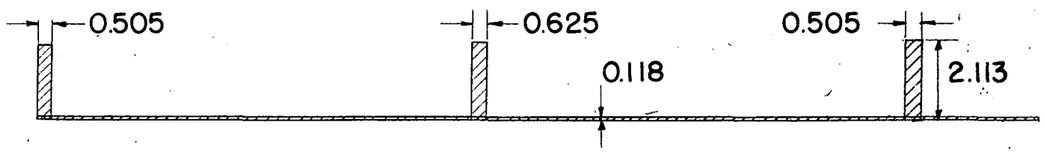

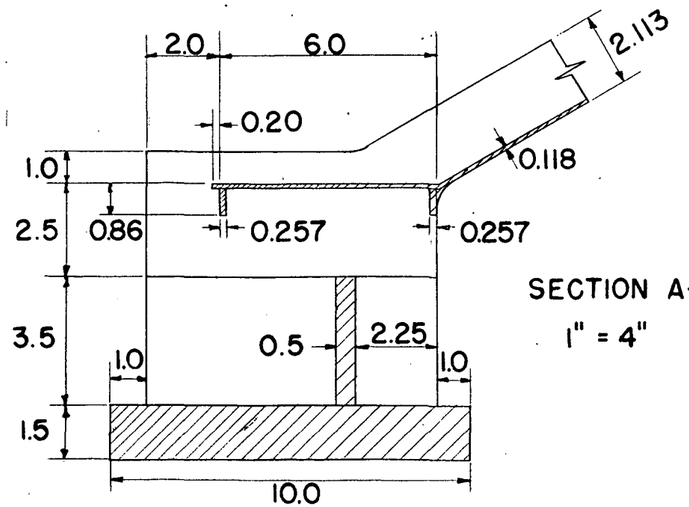

SECTION A-A 1" = 4"

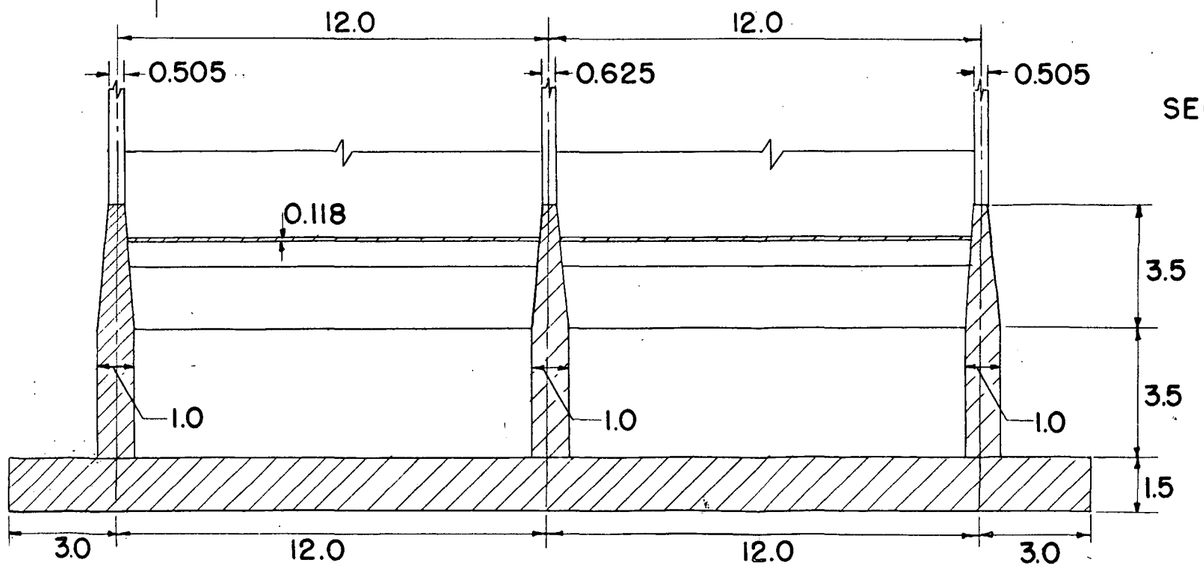

SECTION B-B 1" = 4"

FIG. 10

a.) Outer Rib

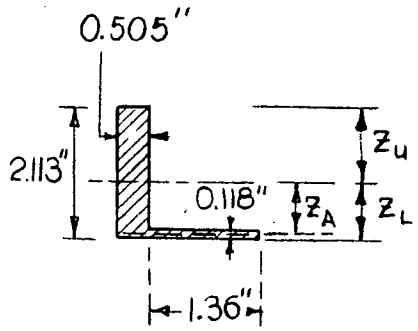

b.) Middle Rib

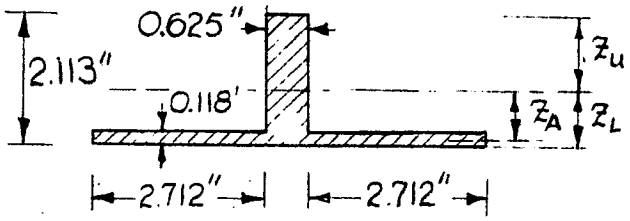

Effective section of the ribs

— Fig 11 —

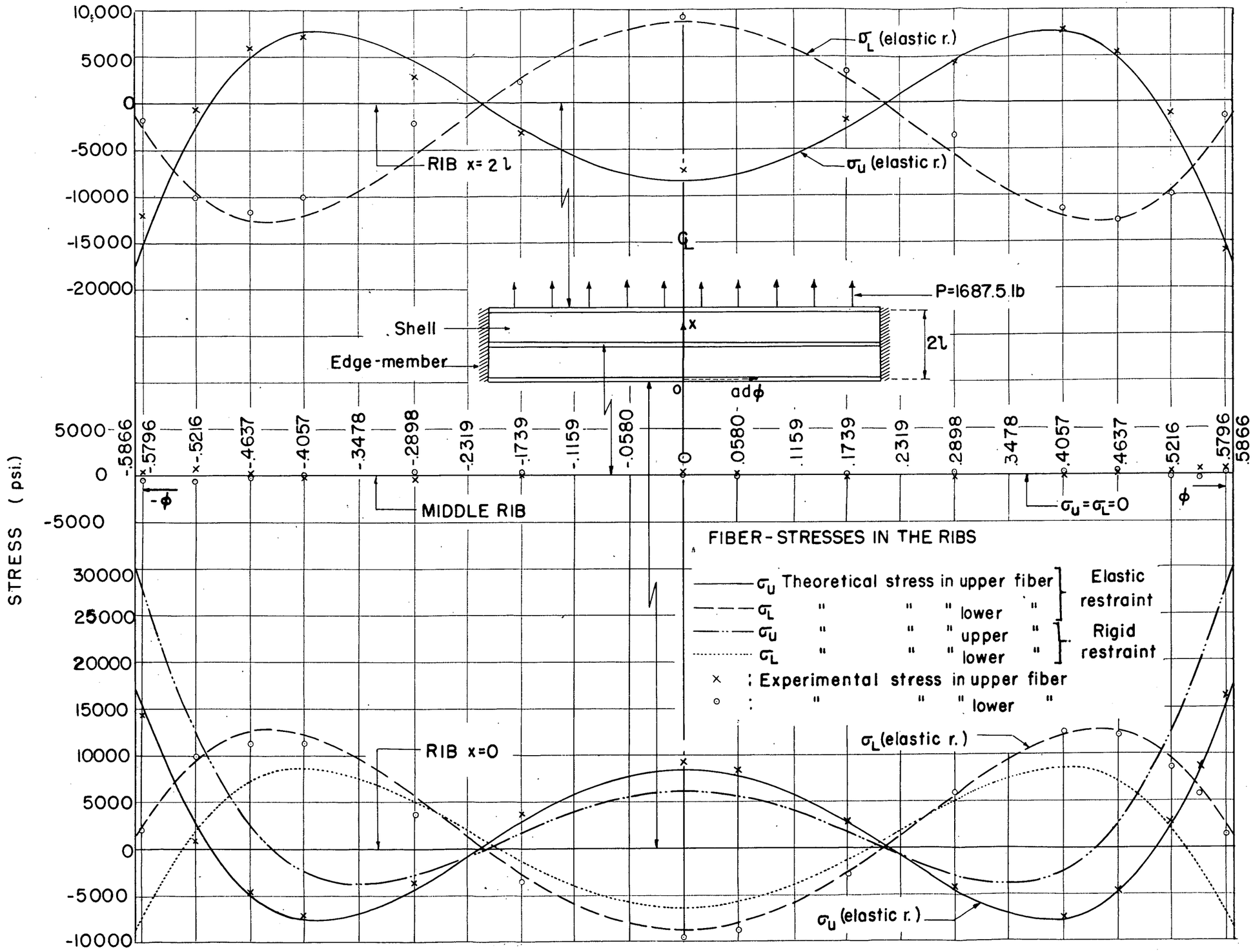

FIBER-STRESS $(\frac{N}{A} \pm \frac{Mz}{I})$ AT UPPER AND LOWER EDGES OF RIBS.

FIG. 12

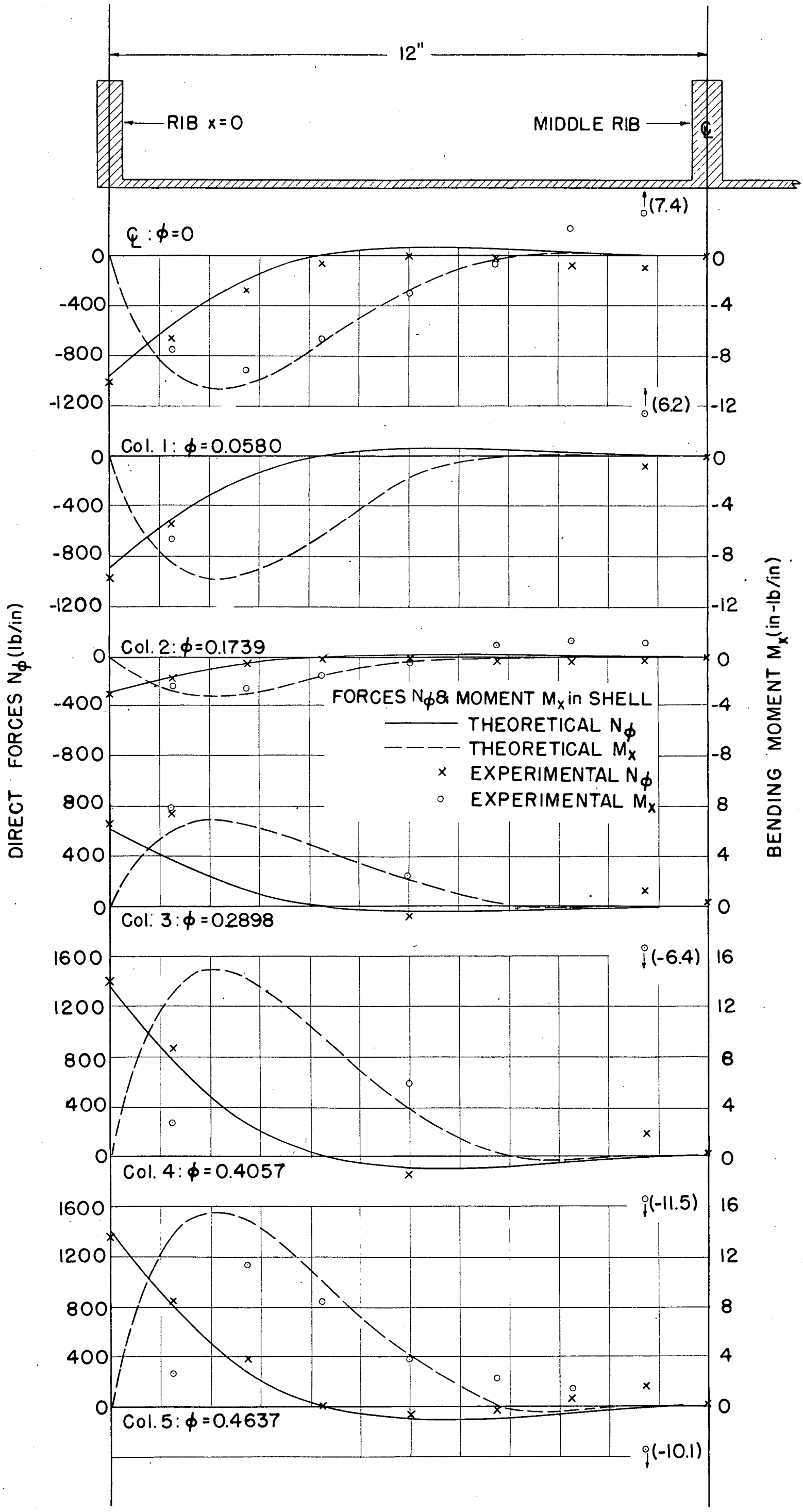

FIG. 13. FORCES N_ϕ AND MOMENT M_x IN SHELL.

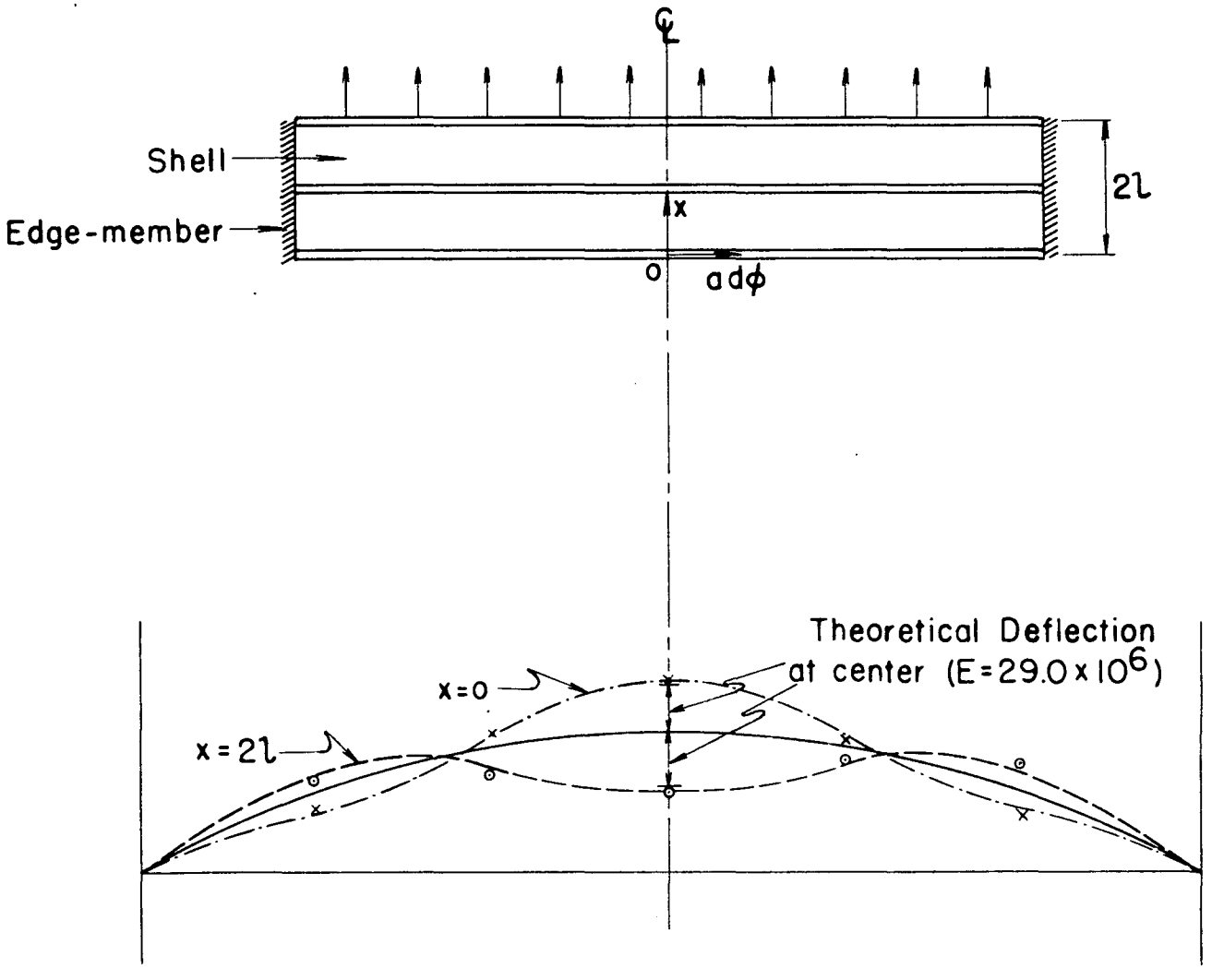

EXPERIMENTAL VERTICAL DEFLECTIONS OF THE OUTER RIBS FOR LATERAL LOADS.

FIG. 14

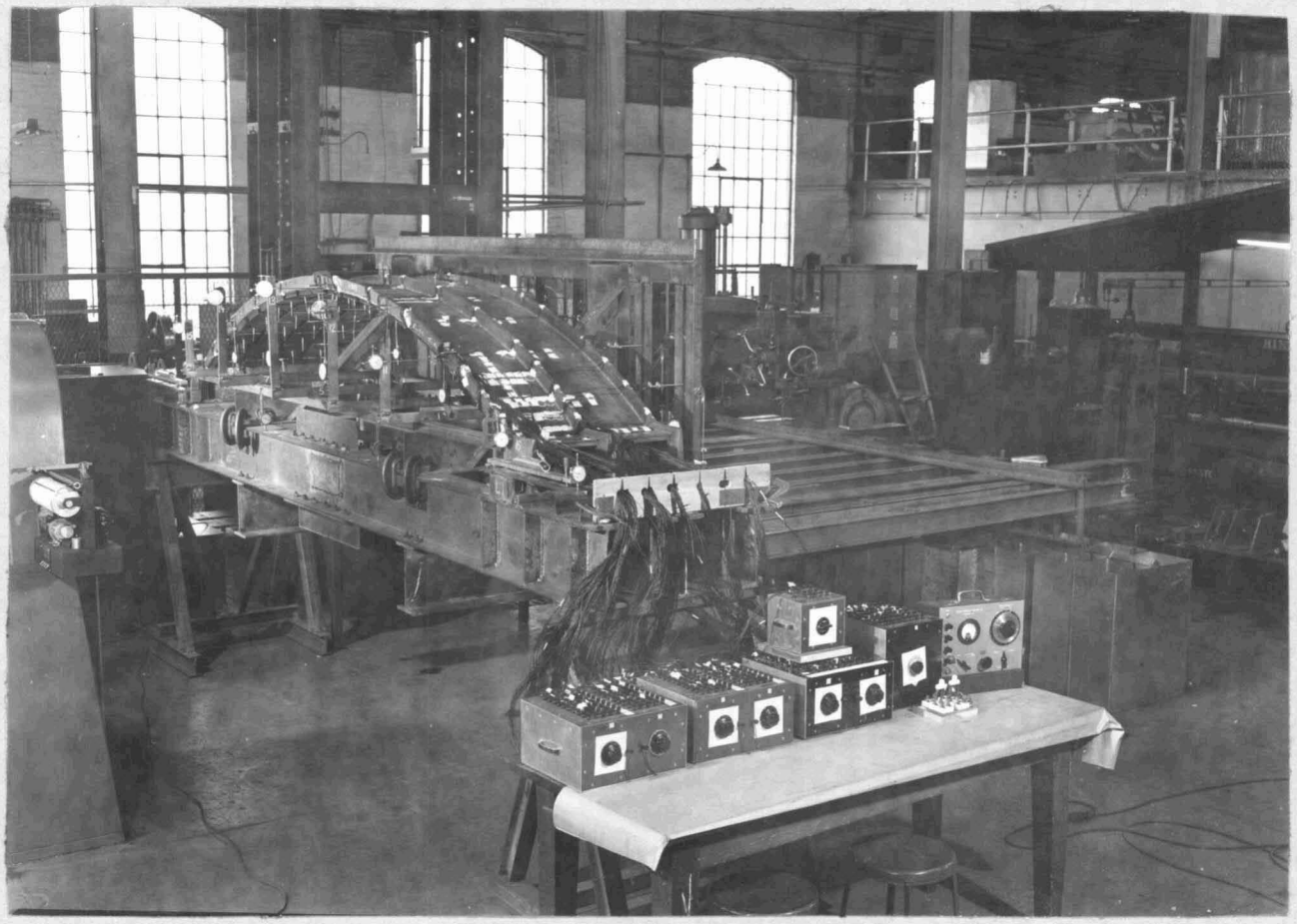

Fig. 15

Actual system:

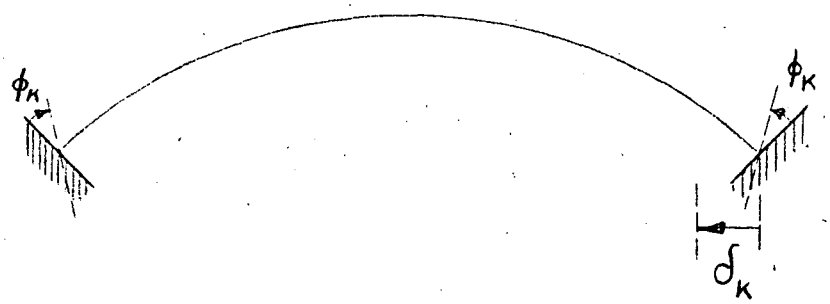

a)

δ_K = horizontal displacement

ϕ_K = end rotation

Base system:

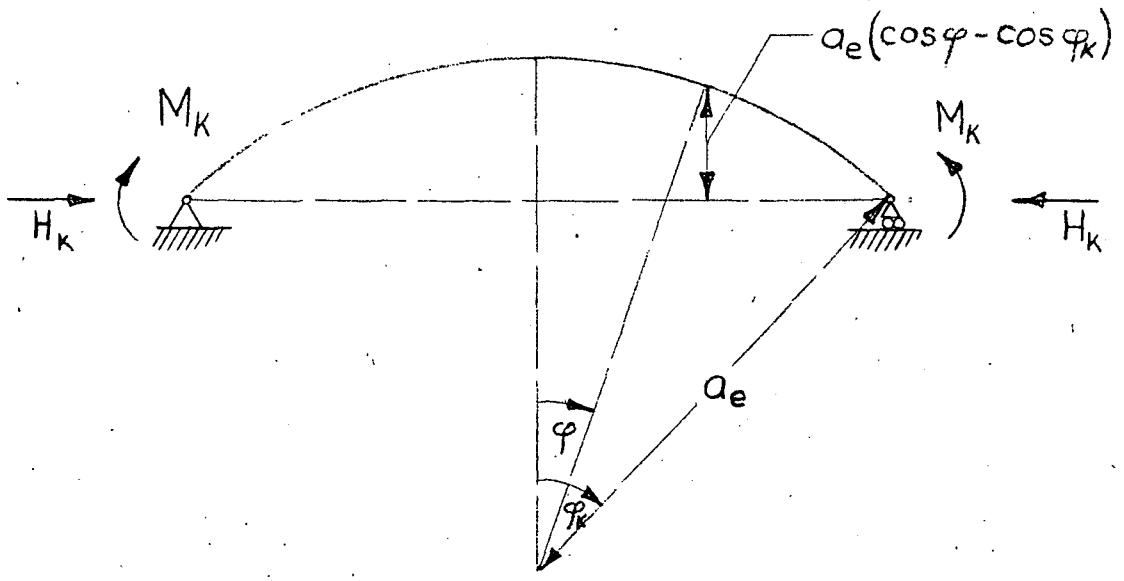

b.) Virtual load system

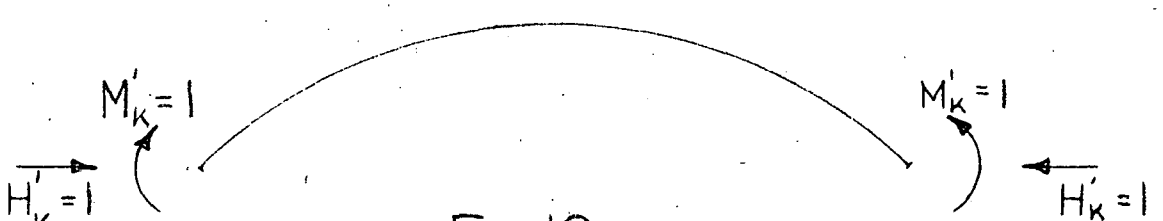

—Fig 16—

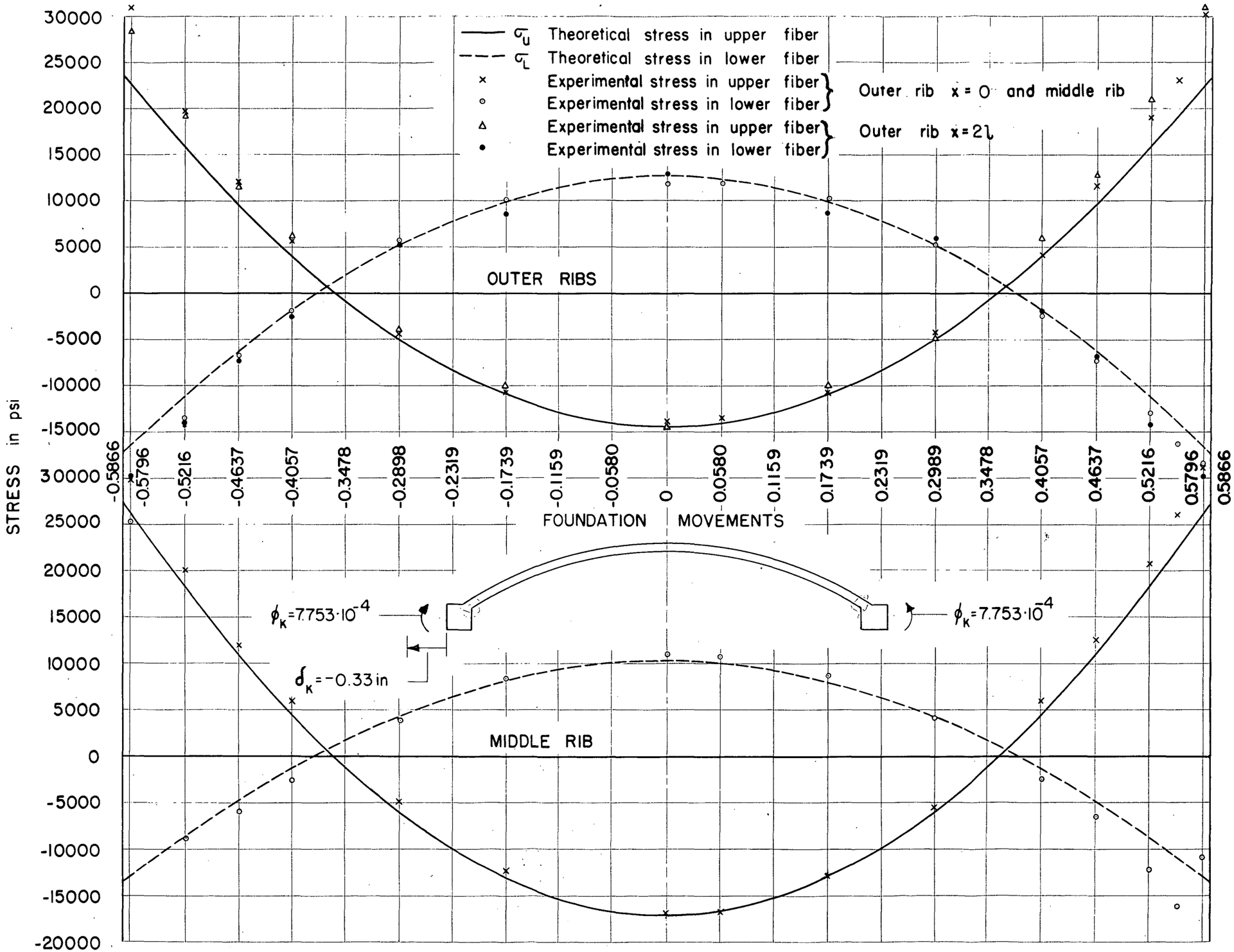
σu Theoretical stress in upper fiber
σL Theoretical stress in lower fiber
Experimental stress in upper fiber
Experimental stress in lower fiber
Outer rib x = 0 and middle rib
Experimental stress in upper fiber
Experimental stress in lower fiber
Outer rib x = 2l
OUTER RIBS
STRESS in psi
30000
25000
20000
15000
10000
5000
0
-5000
-10000
-15000
-20000
-0.5866
-0.5796
-0.5216
-0.4637
-0.4057
-0.3478
-0.2898
-0.2319
-0.1739
-0.1159
-0.0580
0
0.0580
0.1159
0.1739
0.2319
0.2989
0.3478
0.4057
0.4637
0.5216
0.5796
0.5866
FOUNDATION MOVEMENTS
$\phi_K = 7.753 \cdot 10^{-4}$
$\phi_K = 7.753 \cdot 10^{-4}$
$\delta_K = -0.33$ in
MIDDLE RIB

Fig. 17

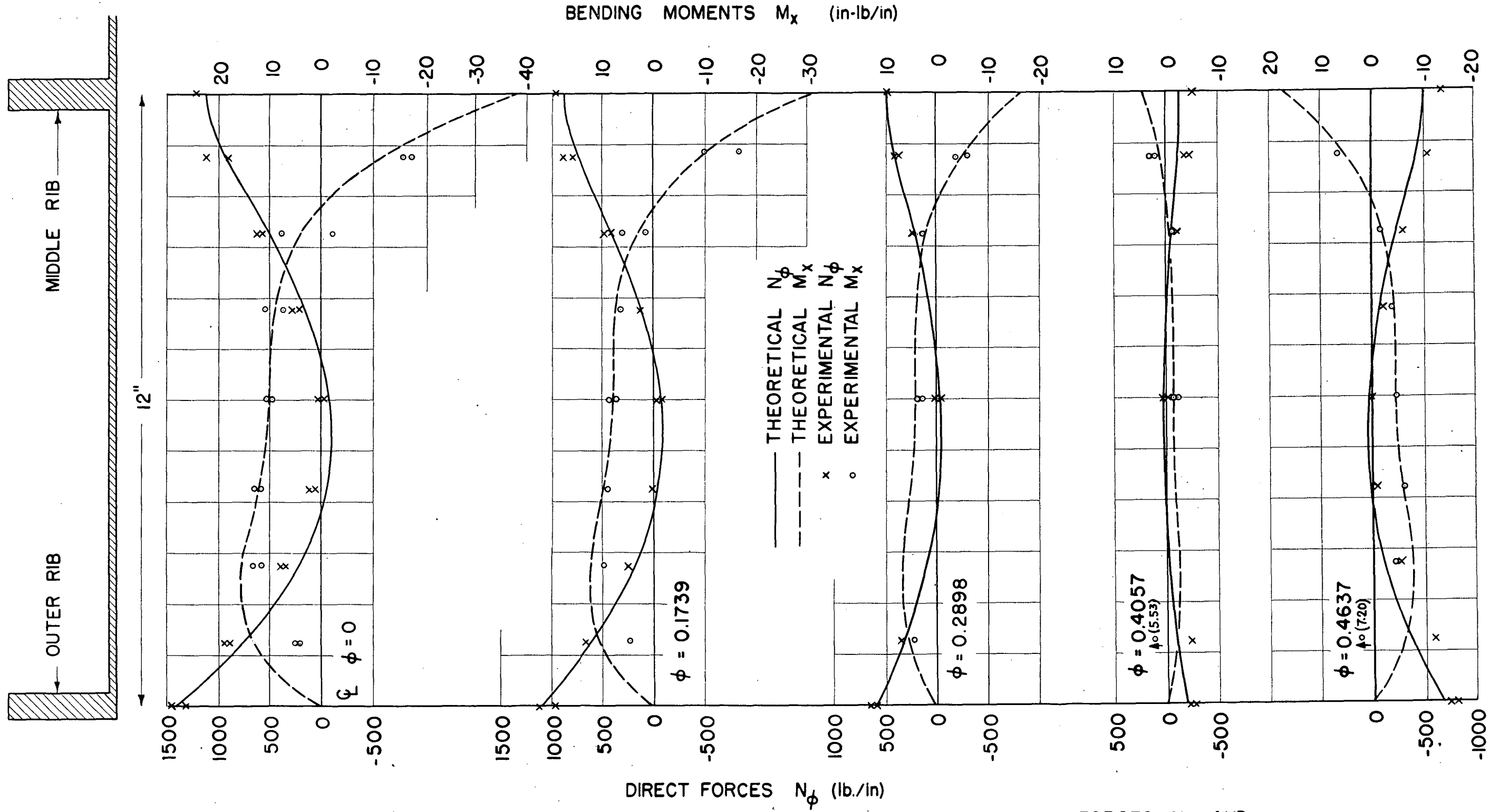

FORCES N_ϕ AND
MOMENTS M_x IN SHELL

Fig 18

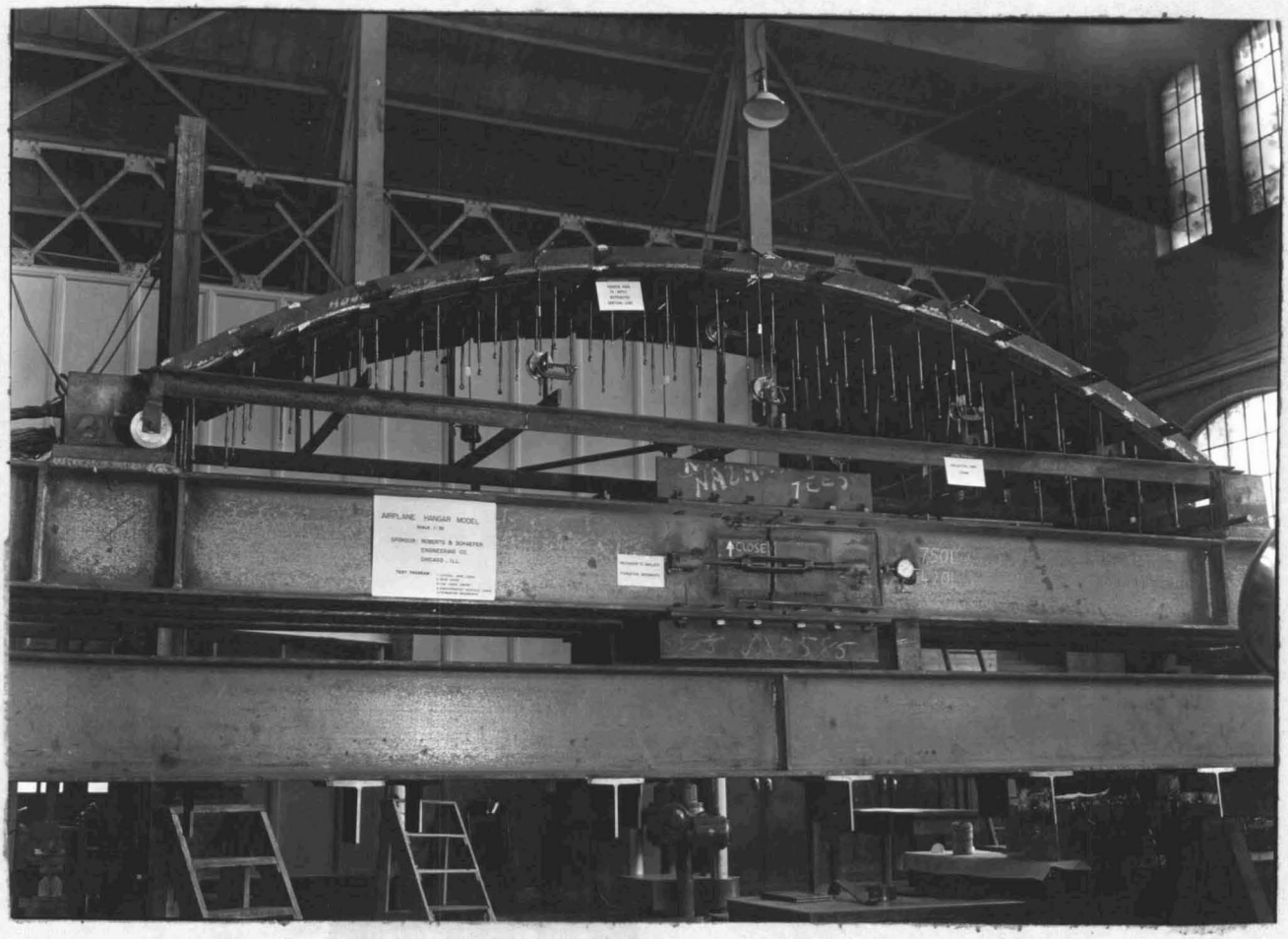
AIRPLANE HANGAR MODEL
SPONSOR: ROBERTS & SCHAEFER
ENGINEERING CO.
CHICAGO, ILL.
CLOSE

Fig. 19